ARTICLE

doi:10.1038/nature17173

High-fat diet enhances stemness and tumorigenicity of intestinal progenitors

Semir Beyaz[1,2]*, Miyeko D. Mana[1]*, Jatin Roper[1,3]*, Dmitriy Kedrin[1,4], Assieh Saadatpour[5], Sue-Jean Hong[6], Khristian E. Bauer-Rowe[1], Michael E. Xifaras[1], Adam Akkad[1], Erika Arias[1], Luca Pinello[5], Yarden Katz[7], Shweta Shinagare[1], Monther Abu-Remaileh[1,6], Maria M. Mihaylova[1,6], Dudley W. Lamming[8], Rizkullah Dogum[1], Guoji Guo[2], George W. Bell[6], Martin Selig[4], G. Petur Nielsen[4], Nitin Gupta[9], Cristina R. Ferrone[4], Vikram Deshpande[4], Guo-Cheng Yuan[5], Stuart H. Orkin[2], David M. Sabatini[1,6,7] & Ömer H. Yilmaz[1,4,7]

Little is known about how pro-obesity diets regulate tissue stem and progenitor cell function. Here we show that high-fat diet (HFD)-induced obesity augments the numbers and function of *Lgr5*$^+$ intestinal stem cells of the mammalian intestine. Mechanistically, a HFD induces a robust peroxisome proliferator-activated receptor delta (PPAR-δ) signature in intestinal stem cells and progenitor cells (non-intestinal stem cells), and pharmacological activation of PPAR-δ recapitulates the effects of a HFD on these cells. Like a HFD, *ex vivo* treatment of intestinal organoid cultures with fatty acid constituents of the HFD enhances the self-renewal potential of these organoid bodies in a PPAR-δ-dependent manner. Notably, HFD- and agonist-activated PPAR-δ signalling endow organoid-initiating capacity to progenitors, and enforced PPAR-δ signalling permits these progenitors to form *in vivo* tumours after loss of the tumour suppressor *Apc*. These findings highlight how diet-modulated PPAR-δ activation alters not only the function of intestinal stem and progenitor cells, but also their capacity to initiate tumours.

The mammalian intestine is known to respond to dietary signals[1]. *Lgr5*$^+$ intestinal stem cells (ISCs) remodel intestinal composition in response to diet-induced cues by adjusting their production of daughter stem cells and (non-ISC, transit-amplifying cells) progenitor cells, the latter of which differentiate into the diverse cell types of the intestine[1–3]. The *Lgr5*$^+$ ISCs reside at the base of intestinal crypts adjacent to Paneth cells, which are a central component of the ISC niche and regulate stem-cell biology in response to calorie-restricted diets[1,4].

Although important epidemiological and rodent studies link obesity to colon cancer incidence[3,5–7], little is known about how the adaptation of stem and progenitor cells to pro-obesity diets alters the potential of these cells to initiate tumours[3]. In the mouse intestine, *Lgr5*$^+$ ISCs serve as the cell-of-origin for the precancerous adenomatous lesions caused by loss of the *Apc* tumour suppressor gene; yet, it is unclear whether this occurs in the context of obesity-linked intestinal tumorigenesis[8,9]. Here, we interrogate how long-term HFD-induced obesity influences intestinal stem and progenitor cell function and the cellular origins of intestinal dysplasia.

HFD boosts ISC counts and crypt function

To assess the effects of obesity on intestinal homeostasis, we maintained mice on a long-term HFD (60% fat diet; Extended Data Fig. 1o) for 9–14 months, which is sufficient to observe many of the metabolic phenotypes associated with obesity[10,11]. Consistent with previous reports, HFD-fed mice gained considerably more mass than their standard chow-fed counterparts (Extended Data Fig. 1a). While the small intestines from HFD-fed mice were shorter in length (Extended Data Fig. 1c) and weighed less (Extended Data Fig. 1b), there was no change in the density of crypt–villous units (Extended Data Fig. 1d) or the number of apoptotic cells (Extended Data Fig. 1n). Morphologically, a HFD led to a mild reduction in villi length (Extended Data Fig. 1g), an associated decrease in villous enterocyte numbers (Extended Data Fig. 1f), and an increase in crypt depth (Extended Data Fig. 1e). A HFD did not change the numbers of chromogranin A$^+$ enteroendocrine cells or Alcian blue$^+$ goblet cells per crypt–villus unit of the small intestine (Extended Data Fig. 2a–d).

To address how a HFD affects the frequency of ISCs, we performed *in situ* hybridization for olfactomedin 4 (*Olfm4*), a marker expressed by the *Lgr5*$^+$ ISCs[12]. Compared to mice fed a standard chow diet, those on a HFD had a 50% increase in the number of *Olfm4*$^+$ ISCs (Fig. 1a and Extended Data Fig. 1l). By contrast, a HFD reduced cryptdin 4$^+$ (*Crp4*$^+$, also known as *Defa4*$^+$) niche Paneth cell numbers by 23% (Fig. 1a and Extended Data Fig. 1m). These observations lead to two conclusions: first, a HFD enhances ISC numbers and self-renewal (for example, deeper crypts with more *Olfm4*$^+$ ISCs) at the expense of differentiation (shorter and less cellular villi); and, second, the increase in ISCs occurs despite a reduction in Paneth cell numbers, raising the possibility that under a HFD, ISCs adjust to fewer interactions from their Paneth cell niche.

Given that ISC numbers and proliferation (Fig. 1b, Extended Data Figs 1h–k and 3f and Supplementary Information) increase in a HFD, we asked whether a HFD also boosts intestinal regeneration. Using an *in vitro* approach, we assessed the ability of isolated intestinal crypts to form organoid bodies in 3-D culture. These organoids recapitulate the epithelial architecture and cellular diversity of the mammalian intestine and are a proxy for ISC activity, as only stem cells can initiate and maintain these structures long-term[1,13]. HFD-derived crypts from the small intestine and colon were more likely to initiate mini-intestines in

[1]The David H. Koch Institute for Integrative Cancer Research at MIT, Department of Biology, MIT, Cambridge, Massachusetts 02139, USA. [2]Division of Hematology/Oncology, Boston Children's Hospital and Department of Pediatric Oncology, Dana-Farber Cancer Institute, Howard Hughes Medical Institute, Harvard Stem Cell Institute, Harvard Medical School, Boston, Massachusetts 02115, USA. [3]Division of Gastroenterology and Molecular Oncology Research Institute, Tufts Medical Center, Boston, Massachusetts 02111, USA. [4]Departments of Pathology, Gastroenterology, and Surgery, Massachusetts General Hospital and Harvard Medical School, Boston, Massachusetts 02114, USA. [5]Department of Biostatistics and Computational Biology, Dana-Farber Cancer Institute and Harvard T. H. Chan School of Public Health, Boston, Massachusetts 02115, USA. [6]Whitehead Institute for Biomedical Research, Howard Hughes Medical Institute, Department of Biology, MIT, Cambridge, Massachusetts 02142, USA. [7]Broad Institute of Harvard and MIT, Cambridge, Massachusetts 02142, USA. [8]Department of Medicine, University of Wisconsin-Madison, Madison, Wisconsin 53705, USA. [9]Division of Digestive Diseases, University of Mississippi Medical Center, Jackson, Missisippi 39216, USA.
*These authors contributed equally to this work.

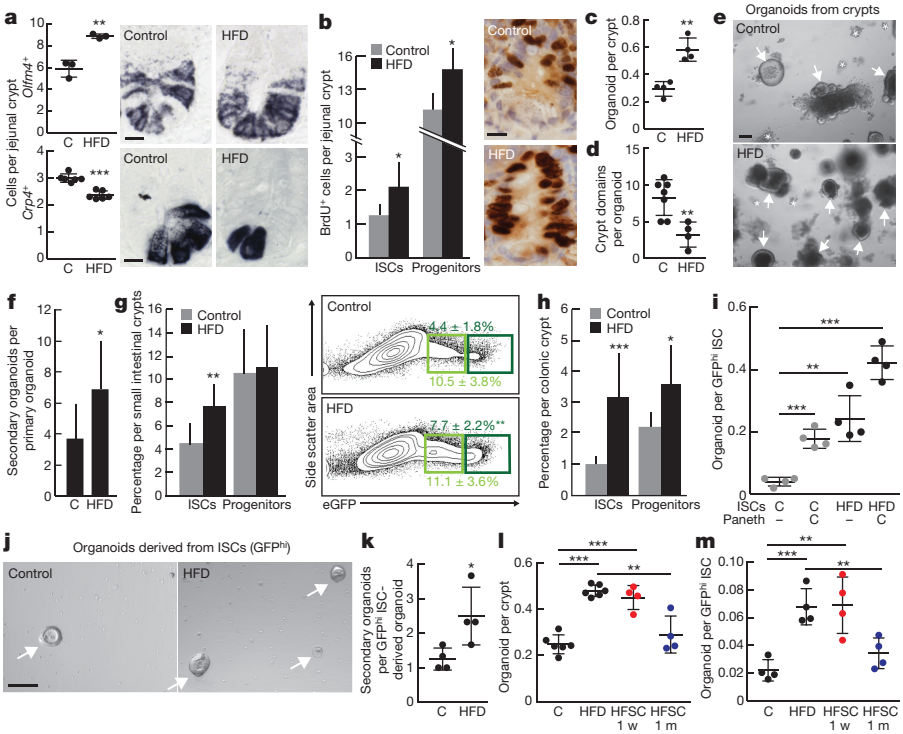

Figure 1 | HFD augments ISC numbers and function. **a**, Quantification of *Olfm4*$^+$ ISCs ($n=3$) and *Crp4*$^+$ Paneth cells ($n=6$) in the proximal jejunum of control (C) and HFD-fed mice by *in situ* hybridization. **b**, BrdU incorporation in ISCs (crypt base columnar cells) and progenitors (transit-amplifying cells) after a 4-h pulse ($n=6$). **c**–**e**, Organoid per crypt (**c**, $n=4$) and crypt domain (**d**, $n=7$) quantification from control and HFD-fed mice (**d**, $n=4$). Representative images: day-7 organoids (**e**). Arrows denote organoids; asterisks denote aborted crypts. **f**, Number of secondary organoids per dissociated crypt-derived primary organoids ($n=9$ primary organoids, 3 primary organoids per sample were individually subcloned in 3 independent experiments). **g**, **h**, Frequencies of ISCs (Lgr5-GFP^{hi}, dark green) and progenitors (Lgr5-GFP^{low}, light green) in the entire small intestine (**g**, $n=10$) and colon (**h**, $n=8$) as measured by flow cytometry. **i**, **j**, Organoid-initiating capacity of control and HFD ISCs cultured with/without Paneth cells (**i**, $n=4$). Representative images: day-5 primary organoids (arrows, **j**). **k**, Number of secondary organoids per dissociated ISC-derived primary organoid ($n=4$). **l**, **m**, Crypts (**l**) and ISCs (**m**) isolated from HFD-fed mice that were reverted to a standard chow diet (HFSC) retained augmented organoid-forming capacity for 1 week (w) (red; $n=4$) but not for 1 month (m) (blue; $n=4$) when compared to their HFD counterparts ($n=6$ crypts, $n=4$ ISCs). Unless otherwise indicated, data are mean ± s.d. from n independent experiments. $^*P<0.05$, $^{**}P<0.01$, $^{***}P<0.001$ (Student's t-tests). Scale bars, 20 μm (**a**, **b**) and 100 μm (**e**, **j**). Histological analysis: **a**, *Olfm4*: 10 crypts per group, *Crp4*: 50 crypts per group; **b**, 50 crypts per group in each experiment.

culture than those from controls (Fig. 1c, e and Extended Data Fig. 3j). Furthermore, these organoids were more cystic (that is, less differentiated[14]) in structure and contained fewer crypt domains (Fig. 1d). When sub-cloned, HFD-derived primary organoids generated more secondary organoids (Fig. 1f and Extended Data Fig. 3k). Consistent with these findings, HFD crypt-derived organoids had higher frequencies of *Lgr5*$^+$ ISCs compared to controls (Extended Data Fig. 4a, d, e), and possessed diverse intestinal cell types, such as Paneth cells, ISCs, enteroendocrine cells and goblet cells (Extended Data Fig. 4b–f).

To determine whether a HFD also augments crypt regeneration *in vivo*, we performed a clonogenic microcolony assay to test for ISC activity[1,15]. After administration of a lethal dose of irradiation, HFD-fed mice manifested increased numbers of surviving, proliferating crypts (Ki67$^+$ cells per crypt) that possessed more *Olfm4*$^+$ ISCs per unit length of intestine relative to controls (Extended Data Fig. 2e–g). These data support the notion that a HFD boosts the numbers and regenerative capacity of ISCs *in vitro* and *in vivo*.

HFD reduces the niche dependence of ISCs

To assess the effects of a HFD on ISCs and progenitors, we used *Lgr5-EGFP-IRES-CreERT2* knock-in mice for the quantification and isolation of green fluorescent protein (GFP)-expressing ISCs (Lgr5-GFP^{hi}) and progenitor cells (Lgr5-GFP^{low})[2]. Compared to controls, mice on a HFD had an increased frequency of Lgr5-GFP^{hi} ISCs in the small intestine (Fig. 1g) and colon (Fig. 1h and Extended Data Fig. 3g).

The opposing effects of a HFD on ISC and Paneth cell numbers led us to ask whether a HFD alters ISC function and niche dependence. We assayed the clonogenic potential of ISCs from control and HFD-fed mice either alone or in combination with the niche Paneth cells[1]. Consistent with earlier studies[1,4,13], control ISCs by themselves inefficiently formed organoids, but robustly formed organoids when co-cultured with Paneth cells (Fig. 1i). Surprisingly, HFD-derived ISCs alone (without Paneth cells) had an increased capacity to initiate organoids with multilineage differentiation and more secondary organoids than control ISCs (Fig. 1i–k and Extended Data Fig. 4h, i, l, m). Co-culture with Paneth cells further increased the organoid-initiating activity of HFD ISCs (Fig. 1i). Organoids derived from control and HFD ISCs alone effectively produced Paneth cells within 24 h of culture (Extended Data Fig. 4j, k). Furthermore, crypts and ISCs isolated from mice that had been on a HFD, but were returned to a standard chow diet, retained an enhanced capacity to initiate organoids for more than 7 days but less than 4 weeks, indicating that the effects of a HFD are reversible (Fig. 1l, m). These data, together with the observation that a HFD uncouples the *in vivo* expansion of ISCs from their Paneth cell niche, suggest ISCs undergo autonomous changes in response to a HFD that poise them for niche-independent growth in the organoid assay.

Fatty acids drive organoid self-renewal

To address whether dietary constituents of the HFD can recapitulate aspects of the HFD-evoked stem-cell phenotype, we expanded control organoids in crypt media supplemented with palmitic acid, a main component of the HFD[16]. Treatment with palmitic acid did not alter the clonogenic potential of control crypts in primary culture

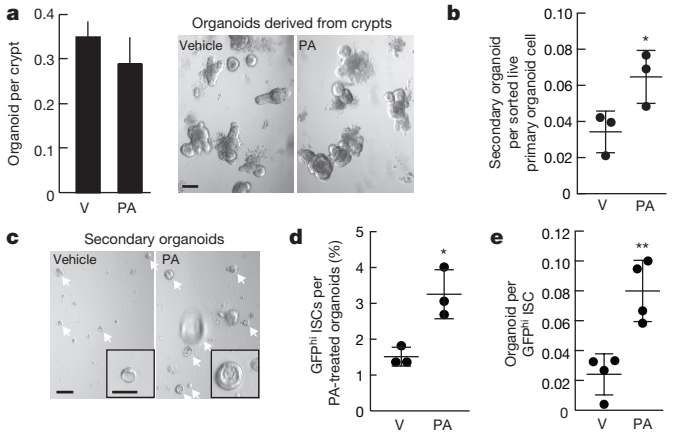

Figure 2 | *Ex vivo* exposure of intestinal organoids to palmitic acid recapitulates aspects of a HFD. a, Clonogenicity of naive crypts cultured with 30 μM palmitic acid (PA) in primary organoid cultures ($n = 5$). Representative images: day-4 organoids. V, vehicle. **b**, **c**, Secondary organoid formation of 1,000 sorted live primary organoid cells after 4 weeks of 30 μM palmitic acid treatment (**b**, $n = 3$). Representative images: day-4 secondary organoids (arrows, **c**). **d**, **e**, Frequency (**d**) and organoid initiation (**e**) of ISCs (Lgr5-GFP^{hi}) after 4 weeks of 30 μM palmitic acid exposure (**d**, $n = 3$; **e**, $n = 4$). Unless otherwise indicated, data are mean ± s.d. from n independent experiments. $^*P < 0.05$, $^{**}P < 0.01$ (Student's t-tests). Scale bars, 100 μm (**a**, **c**) and 50 μm (**c**, inset).

(Fig. 2a). However, as observed with organoids from HFD-fed mice, primary organoids exposed *ex vivo* to palmitic acid gave rise to more secondary organoids than controls (Fig. 2b, c and Extended Data Fig. 5a). Consistent with these findings, organoids treated with palmitic acid possessed nearly twofold more *Lgr5*$^+$ ISCs (Fig. 2d and Extended Data Fig. 5b), and manifested reduced niche dependence in the organoid assay (Fig. 2e). Similar results were obtained with other fatty acids such as oleic acid and a lipid mixture in mouse and human intestinal organoids (Fig. 3h–k and Extended Data Fig. 5c–f). These findings indicate that key dietary constituents of a HFD are sufficient to recapitulate aspects of the *in vivo* HFD stem-cell phenotype.

HFD acts through PPAR-δ in ISCs

To gain mechanistic insight into how HFD mediates these effects, we performed messenger RNA sequencing on isolated Lgr5-GFP^{hi} ISCs and Lgr5-GFP^{low} progenitor cells from control and HFD-fed mice, respectively (Extended Data Fig. 6p). Gene set enrichment analysis (GSEA) pathway and transcription factor binding motif analyses revealed enrichment for transcriptional targets and binding motifs of the nuclear receptor peroxisome proliferator-activated receptor (PPAR) family and PPAR heterodimeric binding partners liver/retinoid X receptor[17–19] (LXR/RXR; Extended Data Fig. 6c, d). Three members (α, δ and γ) comprise the PPAR family[17]; among these, PPAR-δ (*Ppard*) is the predominant one expressed in intestinal stem and progenitor cells at the mRNA level in control and HFD-fed mice (Extended Data Fig. 6a, b). Therefore, we focused our attention on PPAR-δ and its potential role in coupling a HFD to ISC function.

Although PPAR-δ expression itself did not substantially increase (Extended Data Fig. 6a, b), the HFD robustly induced expression of many of its target genes at the mRNA levels in both the small intestine (Extended Data Fig. 6e) and colon (Extended Data Fig. 3h). The induction of the PPAR-δ program was verified at the protein level in ISCs and progenitors (Fig. 3a). To address functionally whether engagement of a PPAR-δ program mimics the HFD, we administered the PPAR-δ agonist GW501516 for 4 weeks to *Lgr5-EGFP-IRES-CreERT2* mice[20,21]. Treatment led to strong induction of PPAR-δ target proteins in ISCs and progenitors (Fig. 3a). Furthermore, agonist-activated PPAR-δ signalling augmented the *in vivo* frequencies of *Olfm4*$^+$ and *Lgr5*$^+$ ISCs (Fig. 3b, e and Extended Data Fig. 6f) and proliferation of stem and progenitors cells (Fig. 3c), but had no effect on Paneth cell numbers (Fig. 3b and Extended Data Fig. 6g). Notably, small intestinal (Fig. 3d) and colonic (Extended Data Fig. 3l, m) crypts from agonist-treated mice initiated more organoids than those from vehicle-treated mice. Similar to ISCs from HFD-fed mice, ISCs derived from agonist-treated mice were more effective at Paneth cell-independent organoid-initiation than their control counterparts (Fig. 3f). In addition, organoids exposed to the PPAR-δ agonist had more *Lgr5*$^+$ ISCs (Fig. 3g) and more self-renewing capacity in secondary assays (Fig. 3i). These data indicate that sustained PPAR-δ signalling largely recapitulates the effects of a HFD on ISC function.

Because *ex vivo* fatty acids mimic aspects of a HFD, we asked whether this phenomenon occurs through PPAR-δ signalling. Like a HFD, we observed that *ex vivo* exposure of mouse and human organoids to fatty acids evokes a robust PPAR-δ program (Extended Data Figs 5g–j and 6h). To assess the necessity of PPAR-δ in this response to fatty acids, we generated tamoxifen-inducible, intestine-specific *Ppard* conditional mice (Extended Data Fig. 6i, j). Acute ablation of *Ppard* in the intestine had no noticeable effects on the numbers, proliferation or function of ISCs and progenitor cells (Fig. 3h and Extended Data Fig. 6i–n). However, loss of *Ppard* blocked both the self-renewal enhancing effects of fatty acids and PPAR-δ agonist (Fig. 3i, j), as well as the induction of PPAR-δ target gene expression in secondary organoid assays (Extended Data Fig. 6o). These findings demonstrate that PPAR-δ mediates fatty-acid-driven organoid self-renewal.

HFD and PPAR-δ raise β-catenin activity

Because HFD and PPAR-δ activation confer increased stem-cell function, we asked whether these interventions regulate the Wnt/β-catenin pathway, which is required for ISC maintenance[2,22]. First, we observed more nuclear β-catenin, a proxy for its activity, in sorted ISCs and progenitors and on intestinal sections from HFD and PPAR-δ agonist-treated mice compared to controls (Extended Data Fig. 7c–i). Second, crypts from HFD and PPAR-δ agonist-treated mice required less exogenous Wnt for organoid maintenance than controls (Fig. 4a, b). Lastly, we found that increased levels of nuclear β-catenin associate with PPAR-δ in HFD crypts (Extended Data Fig. 7j–l).

To address how a HFD and agonist-activated PPAR-δ influence β-catenin transcriptional activity, we performed microfluidic-based multiplexed single-cell quantitative reverse transcription PCR (qRT–PCR) using primers for a curated list of known β-catenin target genes that includes ISC markers (Supplementary Table 2 and Extended Data Fig. 8a, d). While a HFD did not alter expression of stem-cell signature genes (that is, *Lgr5*) that differ between stem and progenitor cells[23,24] (Extended Data Fig. 8b, e, g, h), it evoked expression of a subset of β-catenin target genes such as *Bmp4*, *Jag1*, *Jag2* and *Edn3* in ISCs and progenitors (Fig. 4c, e, Extended Data Figs 3i and 8c, f, i, j and Supplementary Information). Single-cell qRT–PCR analysis confirmed that agonist-activated PPAR-δ also induced transcription of *Bmp4*, *Jag1*, *Jag2* and *Edn3* in ISCs and progenitors (Fig. 4d, f). We further validated *Jag1* expression by single-molecule *in situ* hybridization and found that it was broadly expressed within HFD (Extended Data Fig. 8k) and PPAR-δ agonist-treated crypts (Extended Data Fig. 8l). Moreover, in response to *in vitro* fatty acids, PPAR-δ was required for the induction of *Jag1* and *Jag2* in secondary organoids (Extended Data Fig. 6o). Collectively, these results support a model in which a HFD activates a PPAR-δ-mediated subset of β-catenin target genes in ISCs and progenitor cells.

To interrogate whether a similar program exists in an alternative model of obesity, we assessed how the intestine adapts to obesity in leptin receptor deficient (*db/db*) mice—an obesity model that develops on a standard diet. Overall, we found that intestinal adaptation in the *db/db* obesity model was mostly opposite to what we observed in HFD-fed mice (Extended Data Fig. 9 and Supplementary Information). Such differences highlight that, even in obesity, diet affects ISC and progenitor biology.

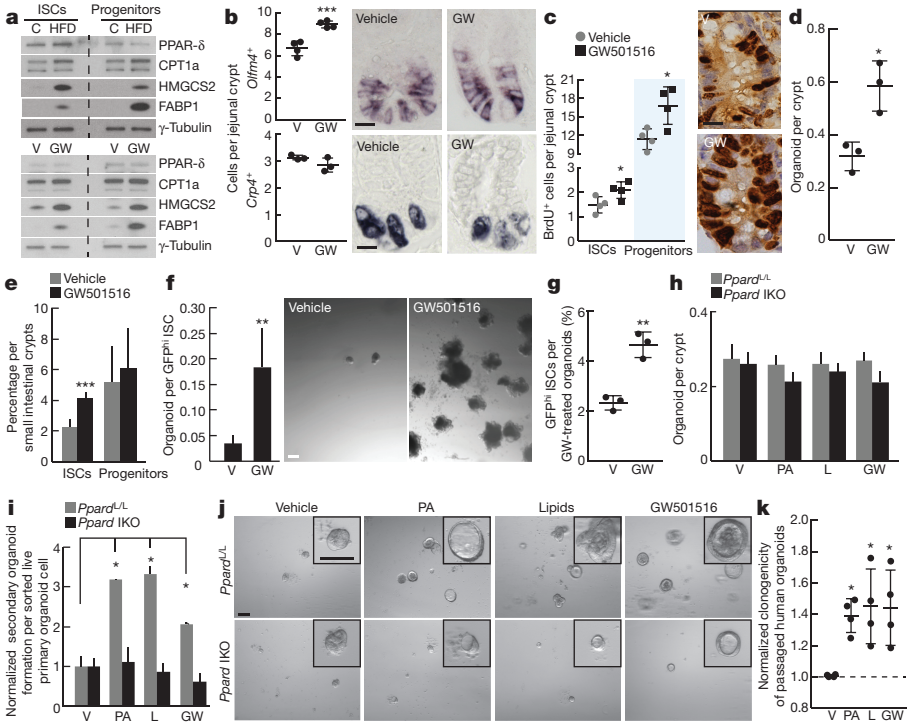

Figure 3 | Activated PPAR-δ in ISCs mediates the effects of a HFD. **a**, Immunoblots of PPAR-δ target proteins in flow-sorted ISCs (Lgr5-GFP^{hi}) and progenitors (Lgr5-GFP^{low}) from control, HFD, vehicle and GW501516 (GW) mice ($n=2$). **b**, Quantification of *Olfm4*$^+$ ISCs ($n=4$) and *Crp4*$^+$ Paneth cells ($n=3$) by *in situ* hybridization in proximal jejunal crypts. **c**, BrdU incorporation in ISCs (crypt base columnar cells adjacent to Paneth cells) and progenitors (transit-amplifying cells not adjacent to Paneth cells) after a 4-h pulse ($n=4$). **d**, Organoid per crypt from vehicle- and GW501516-treated mice ($n=3$). **e**, Frequencies of flow-sorted ISCs (Lgr5-GFP^{hi}) and progenitors (Lgr5-GFP^{low}) ($n=5$) from the entire small intestine of vehicle and GW501516-treated mice. **f**, Organoid-initiating capacity of ISCs derived from vehicle and GW501516-treated mice. Representative images: day-12 organoids ($n=5$). **g**, Frequency of ISCs (Lgr5-GFP^{hi}) in organoids after 14 days of *ex vivo* GW501516 exposure ($n=3$). **h–j**, Primary (**h**, $n=5$) and secondary (**i**, **j**, $n=5$; normalized to vehicle) organoid-forming capacity of control (*Ppard*$^{L/L}$ (L, *loxP*)) and *Ppard* intestinal knockout (IKO) mice upon *ex vivo* treatment with vehicle, palmitic acid, lipid mixture (L) and GW501516. Representative images: day-4 secondary organoids (**j**). **k**, Normalized clonogenicity of human-derived intestinal organoids after *ex vivo* treatment with palmitic acid, lipid mixture and GW501516 in secondary culture ($n=4$, see Methods). Unless otherwise indicated, data are mean ± s.d. from *n* independent experiments. $^*P<0.05$, $^{**}P<0.01$, $^{***}P<0.001$ (Student's *t*-tests). Scale bars, 20 μm (**b**, **c**), 200 μm (**f**) and 100 μm (**j**). Histological analysis: **b**, *Olfm4*: 15 crypts per group, *Crp4*: 50 crypts per group; **c**, 50 crypts per group in each experiment. For western blot source data, see Supplementary Fig. 1.

PPAR-δ permits non-ISCs to beget tumours

Somatic stem cells often accumulate the initial mutations that lead to oncogenic transformation[3,8,25–27]. We found that in a HFD there is a greater incidence of spontaneous intestinal low-grade dysplastic lesions (adenomas), carcinomas, or both than in controls (Fig. 5a–c), which may reflect the fact that there are more ISCs in mice on a HFD that can acquire oncogenic mutations. Because HFD-induced PPAR-δ also activates a β-catenin signature in progenitor cells, we proposed that

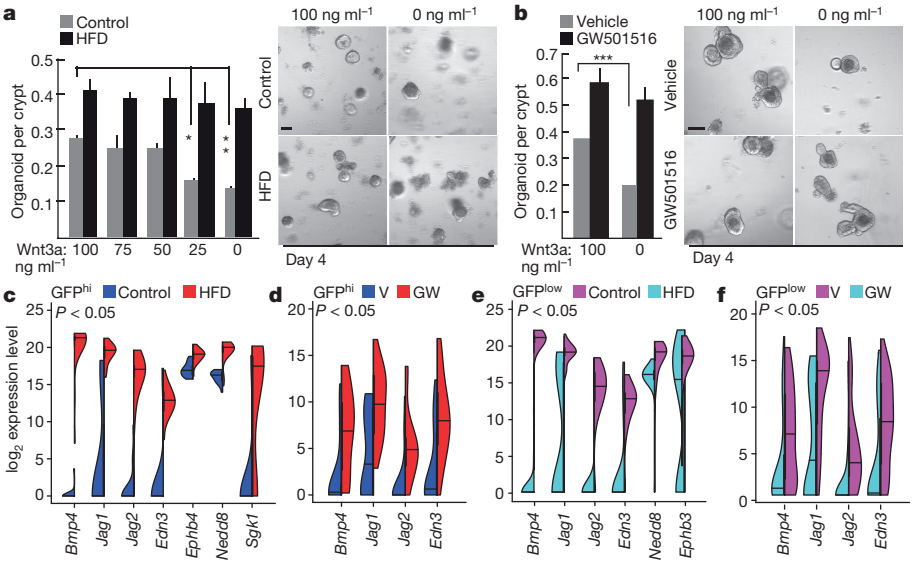

Figure 4 | HFD-induced PPAR-δ signalling induces expression of a subset of β-catenin target genes. a, **b**, Organoid per crypt quantification from HFD-fed (**a**) and GW501516-treated (**b**) mice with indicated concentrations of Wnt3a. Representative images: day-4 organoids ($n=5$). **c–f**, Violin plots for most induced β-catenin target genes in ISCs (Lgr5-GFP^{hi}) from HFD-fed (**c**) and GW501516-treated (**d**) mice (24 single cells per group), and in progenitors (Lgr5-GFP^{low}) from HFD-fed (**e**) and GW501516-treated (**f**) mice (72 single cells per group; see Methods). Unless otherwise indicated, data are mean ± s.d. from *n* independent experiments. $^*P<0.05$, $^{**}P<0.01$, $^{***}P<0.001$ (Student's *t*-tests). Scale bars, 100 μm.

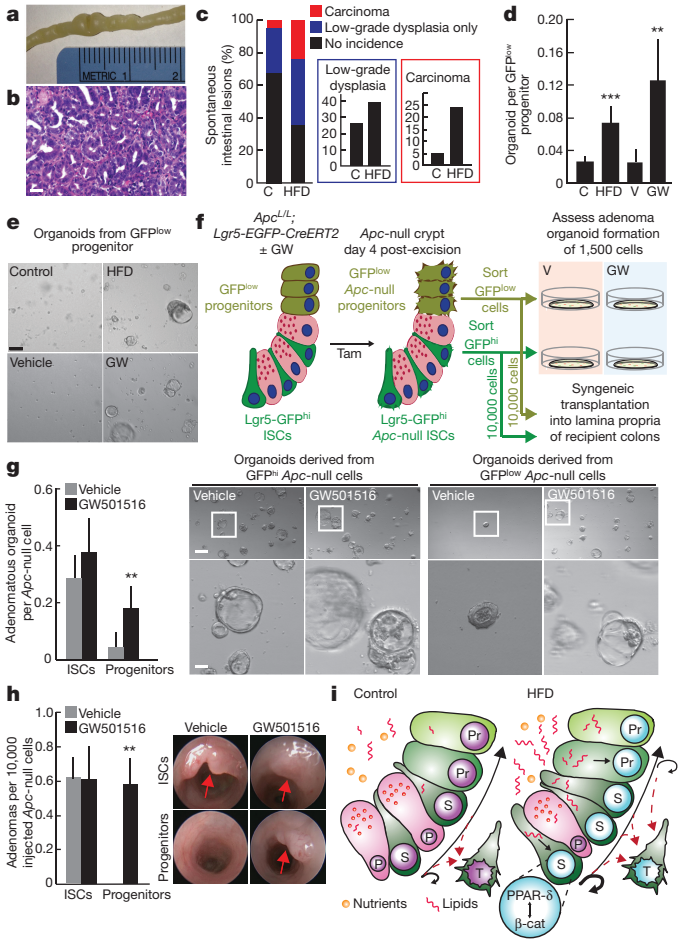

Figure 5 | PPAR-δ activation confers organoid and tumour-initiating capacity to non-stem-cells. a, **b**, Representative spontaneous intestinal tumour from a HFD mouse: gross image (**a**) and microscopic haematoxylin and eosin (H&E) image (**b**). **c**, Incidence of spontaneous intestinal low-grade dysplastic lesions (adenoma) and carcinomas in control ($n = 19$) and HFD ($n = 25$) mice. **d**, **e**, Organoid-initiating capacity of progenitors (Lgr5-GFP^{low}) from HFD ($n = 7$) and GW501516-treated ($n = 5$) mice. Representative images: day-7 organoids (**e**). **f**, Schematic assessing *in vitro* and *in vivo* adenoma-initiating capacity of *Apc*-null ISCs (Lgr5-GFP^{hi}) and progenitors (Lgr5-GFP^{low}) from vehicle- and GW501516-treated mice. Tam, tamoxifen. **g**, Numbers and representative day-5 images of adenomatous organoids from *Apc*-null ISCs (Lgr5-GFP^{hi}) and progenitors (Lgr5-GFP^{low}) treated with/without GW501516 in EN media (EGF and Noggin only) ($n = 6$). **h**, Optical colonoscopy of tumours formed after orthotopic transplantation of 10,000 *Apc*-null ISCs (Lgr5-GFP^{hi}) or *Apc*-null progenitors (Lgr5-GFP^{low}) from vehicle- and GW501516-treated mice ($n = 5$). **i**, Model of intestinal adaptation to HFD: mechanistically, HFD activates a PPAR-δ-mediated program that augments the organoid- and tumour-initiating capacity of intestinal progenitors. A feature of the PPAR-δ program includes induction of a subset of β-catenin target genes. P, Paneth cell; Pr, progenitor cell; S, stem cell, T, tumour cell. Red dotted lines denote *Apc*-null cells with tumour-forming capability. Unless otherwise indicated, data are mean ± s.d. from *n* independent experiments. $^*P < 0.05$, $^{**}P < 0.01$, $^{***}P < 0.001$ (Student's *t*-tests). Scale bars, 50 μm (**b**, **g**, bottom) and 200 μm (**e**, **g**, top).

non-ISC progenitor populations can acquire stem-cell features and contribute to tumour initiation in diet-induced obesity[3,27]. To explore this possibility, we asked whether HFD or agonist-activated PPAR-δ influenced the organoid-initiating capacity of progenitors (non-ISCs). Interestingly, Lgr5-GFP^{low} progenitors, but not terminally differentiated villous enterocytes, from HFD-fed and PPAR-δ-agonist-treated mice formed organoids (Fig. 5d, e and Extended Data Figs 4g and 7a, b), raising the possibility that enforced PPAR-δ signalling in intestinal progenitors not only bestows organoid-initiating capacity but also tumour-initiating potential.

To test this possibility, we generated *Apc*$^{L/L}$; *Lgr5-EGFP-IRES-CreERT2* mice to assess whether pharmacological PPAR-δ activation modifies the tumorigenic capacity of the Lgr5-GFP^{low} progenitors. Injection with tamoxifen leads to *Apc* loss in the Lgr5-GFP^{hi} ISCs, which in turn generates *Apc*-null Lgr5-GFP^{low} progenitors (Extended Data Fig. 10c). Four days after tamoxifen administration, we isolated *Apc*-null Lgr5-GFP^{hi} ISCs and Lgr5-GFP^{low} progenitors from vehicle and PPAR-δ-agonist-treated mice to assess the tumour-forming potential of these populations using separate assays (Fig. 5f, schematic): first, we examined their capacity to give rise to adenomatous organoids in culture; and second, we interrogated the ability of 10,000 sorted stem and progenitor cells to initiate adenomas in syngeneic recipient colons.

We found that *Apc*-null ISCs from PPAR-δ agonist-treated mice were as clonogenic as those from vehicle controls; however, enforced PPAR-δ signalling in *Apc*-null progenitors markedly boosted their ability to form adenomatous organoids (Fig. 5g). Next, we assessed the potential of freshly isolated ISC and progenitor cells to form *in vivo* intestinal adenomas (Fig. 5f, schematic). As in the organoid assay, the PPAR-δ agonist had no additive effect on the ability of *Apc*-null stem cells to form β-catenin$^+$ (*Apc*-null) adenomas (Fig. 5h and Extended Data Fig. 10a, d) compared to vehicle controls. However, enforced PPAR-δ signalling permitted *Apc*-null progenitors, but not their vehicle-treated counterparts, to initiate β-catenin$^+$ (*Apc*-null) adenomas robustly after transplantation into recipient colons (Fig. 5h and Extended Data Fig. 10b, d). These data indicate that PPAR-δ activation enables a subset of non-ISC progenitors to initiate adenomatous growth *in vitro* and *in vivo* (see Supplementary Information).

Discussion

Our data favour a model in which a HFD augments ISC self-renewal and bestows features of stemness (that is, organoid-initiating capacity) on non-stem-cell progenitors by activating PPAR-δ signalling (Fig. 5i). A previous study shows that a different dietary regimen, calorie restriction, increases both stem and Paneth cell numbers and regulates ISC function non-cell autonomously through the Paneth cell niche, with no significant effect on progenitor cell function[1]. By contrast, here we find that a long-term HFD has opposing effects on stem and Paneth cell numbers, and that these stem cells are less dependent on Paneth cells in functional assays. The fact that we find induction of β-catenin targets *Jag1* and *Jag2* (Notch ligands typically elaborated by Paneth cells) in HFD stem and progenitor cells suggests a possible role for Notch signalling. In a HFD, proximate ISCs or progenitor cells may serve as a surrogate source of Notch ligands for *Lgr5*$^+$ ISCs not in direct contact with Paneth cells, enabling them to persist *in vivo* and in the organoid assay. A recent report[28] that PPAR-δ activation in the bone amplifies β-catenin signalling is consistent with our finding that diet-activated PPAR-δ engages a restricted β-catenin program. Notably, genes within the PPAR-δ-activated β-catenin program include *Jag1*, *Jag2* and *Bmp4*, which are often deregulated in early intestinal tumorigenesis[29–31] (Fig. 4c–f).

Recent studies propose that intrinsic and extrinsic factors contribute to cancer risk through the control of stem-cell divisions[25,32]. These models predict that extrinsic factors such as a HFD may raise cancer risk by increasing stem-cell divisions, which are the implicated cell-of-origin for many cancers. Our data (Fig. 5i) and a previous study[33] demonstrate that a HFD augments the numbers and proliferation of ISCs, which may partially account for the increase of intestinal tumours in this model of obesity. Another possibility raised by our results is that a HFD-driven PPAR-δ program also enhances the susceptibility of non-ISCs to undergo oncogenic transformation, thus establishing a larger and more diverse pool of cells capable of initiating tumours. Consistent with this notion, it has been proposed that differentiated cells (non-ISCs) in the background of *Apc*-deficiency

with concurrent activation of oncogenic KRAS and pro-inflammatory NF-κB signalling have the capacity to initiate tumours[9]. Whether and how obesity-related inflammation in a HFD contributes to PPAR-δ signalling and intestinal tumorigenesis is unknown. In our models, we find no evidence that a HFD or its predominant fatty acid constituents activate inflammatory pathways in intestinal crypts[34] or organoids, respectively (Extended Data Fig. 3a–e).

While some previous work indicates that PPAR-δ inhibition may have modest anti-cancer effects[19], sustained PPAR-δ activation and a HFD have been linked to colorectal cancer initiation and progression[7,35–40]. Future studies will need to address whether PPAR-δ inhibition in the setting of a HFD affects tumour initiation and progression. Lastly, it will be important to explore if lean ketogenic diets, which like a HFD are composed largely of fatty acids but with fewer carbohydrates, mimic the pro-regenerative effects of a HFD while minimizing the untoward sequelae of obesity.

Online Content Methods, along with any additional Extended Data display items and Source Data, are available in the online version of the paper; references unique to these sections appear only in the online paper.

Received 22 March 2015; accepted 28 January 2016.

1. Yilmaz, Ö. H. *et al.* mTORC1 in the Paneth cell niche couples intestinal stem-cell function to calorie intake. *Nature* **486,** 490–495 (2012).
2. Barker, N. *et al.* Identification of stem cells in small intestine and colon by marker gene *Lgr5*. *Nature* **449,** 1003–1007 (2007).
3. Mihaylova, M. M., Sabatini, D. M. & Yilmaz, O. H. Dietary and metabolic control of stem cell function in physiology and cancer. *Cell Stem Cell* **14,** 292–305 (2014).
4. Sato, T. *et al.* Paneth cells constitute the niche for Lgr5 stem cells in intestinal crypts. *Nature* **469,** 415–418 (2011).
5. Finucane, M. M. *et al.* National, regional, and global trends in body-mass index since 1980: systematic analysis of health examination surveys and epidemiological studies with 960 country-years and 9.1 million participants. *Lancet* **377,** 557–567 (2011).
6. Calle, E. E. & Kaaks, R. Overweight, obesity and cancer: epidemiological evidence and proposed mechanisms. *Nature Rev. Cancer* **4,** 579–591 (2004).
7. Baltgalvis, K. A., Berger, F. G., Pena, M. M., Davis, J. M. & Carson, J. A. The interaction of a high-fat diet and regular moderate intensity exercise on intestinal polyp development in $Apc^{Min/+}$ mice. *Cancer Prev. Res. (Phila.)* **2,** 641–649 (2009).
8. Barker, N. *et al.* Crypt stem cells as the cells-of-origin of intestinal cancer. *Nature* **457,** 608–611 (2009).
9. Schwitalla, S. *et al.* Intestinal tumorigenesis initiated by dedifferentiation and acquisition of stem-cell-like properties. *Cell* **152,** 25–38 (2013).
10. Eckel-Mahan, K. L. *et al.* Reprogramming of the circadian clock by nutritional challenge. *Cell* **155,** 1464–1478 (2013).
11. Winzell, M. S. & Ahren, B. The high-fat diet-fed mouse: a model for studying mechanisms and treatment of impaired glucose tolerance and type 2 diabetes. *Diabetes* **53** (suppl. 3), S215–S219 (2004).
12. Schuijers, J., van der Flier, L. G., van Es, J. & Clevers, H. Robust Cre-mediated recombination in small intestinal stem cells utilizing the *Olfm4* locus. *Stem Cell Reports* **3,** 234–241 (2014).
13. Sato, T. *et al.* Single Lgr5 stem cells build crypt-villus structures *in vitro* without a mesenchymal niche. *Nature* **459,** 262–265 (2009).
14. Schuijers, J. *et al.* Ascl2 acts as an R-spondin/Wnt-responsive switch to control stemness in intestinal crypts. *Cell Stem Cell* **16,** 158–170 (2015).
15. Marsh, V. *et al.* Epithelial Pten is dispensable for intestinal homeostasis but suppresses adenoma development and progression after *Apc* mutation. *Nature Genet.* **40,** 1436–1444 (2008).
16. Buettner, R. *et al.* Defining high-fat-diet rat models: metabolic and molecular effects of different fat types. *J. Mol. Endocrinol.* **36,** 485–501 (2006).
17. Peters, J. M., Shah, Y. M. & Gonzalez, F. J. The role of peroxisome proliferator-activated receptors in carcinogenesis and chemoprevention. *Nature Rev. Cancer* **12,** 181–195 (2012).
18. Tontonoz, P. & Spiegelman, B. M. Fat and beyond: the diverse biology of PPARγ. *Annu. Rev. Biochem.* **77,** 289–312 (2008).
19. Neels, J. G. & Grimaldi, P. A. Physiological functions of peroxisome proliferator-activated receptor β. *Physiol. Rev.* **94,** 795–858 (2014).
20. Ito, K. *et al.* A PML-PPAR-δ pathway for fatty acid oxidation regulates hematopoietic stem cell maintenance. *Nature Med.* **18,** 1350–1358 (2012).
21. Narkar, V. A. *et al.* AMPK and PPARδ agonists are exercise mimetics. *Cell* **134,** 405–415 (2008).
22. van der Flier, L. G. & Clevers, H. Stem cells, self-renewal, and differentiation in the intestinal epithelium. *Annu. Rev. Physiol.* **71,** 241–260 (2009).
23. van der Flier, L. G. *et al.* Transcription factor achaete scute-like 2 controls intestinal stem cell fate. *Cell* **136,** 903–912 (2009).
24. Muñoz, J. *et al.* The Lgr5 intestinal stem cell signature: robust expression of proposed quiescent '+4' cell markers. *EMBO J.* **31,** 3079–3091 (2012).
25. Tomasetti, C. & Vogelstein, B. Cancer etiology. Variation in cancer risk among tissues can be explained by the number of stem cell divisions. *Science* **347,** 78–81 (2015).
26. Yilmaz, O. H. *et al.* Pten dependence distinguishes haematopoietic stem cells from leukaemia-initiating cells. *Nature* **441,** 475–482 (2006).
27. Meacham, C. E. & Morrison, S. J. Tumour heterogeneity and cancer cell plasticity. *Nature* **501,** 328–337 (2013).
28. Scholtysek, C. *et al.* PPARβ/δ governs Wnt signaling and bone turnover. *Nature Med.* **19,** 608–613 (2013).
29. Rodilla, V. *et al.* Jagged1 is the pathological link between Wnt and Notch pathways in colorectal cancer. *Proc. Natl Acad. Sci. USA* **106,** 6315–6320 (2009).
30. Kumar, S. R. *et al.* Preferential induction of EphB4 over EphB2 and its implication in colorectal cancer progression. *Cancer Res.* **69,** 3736–3745 (2009).
31. Kim, J. S. *et al.* Oncogenic β-catenin is required for bone morphogenetic protein 4 expression in human cancer cells. *Cancer Res.* **62,** 2744–2748 (2002).
32. Wu, S., Powers, S., Zhu, W. & Hannun, Y. A. Substantial contribution of extrinsic risk factors to cancer development. *Nature* **529,** 43–47 (2016).
33. Mah, A. T., Van Landeghem, L., Gavin, H. E., Magness, S. T. & Lund, P. K. Impact of diet-induced obesity on intestinal stem cells: hyperproliferation but impaired intrinsic function that requires insulin/IGF1. *Endocrinology* **155,** 3302–3314 (2014).
34. Johnson, A. M. *et al.* High fat diet causes depletion of intestinal eosinophils associated with intestinal permeability. *PLoS ONE* **10,** e0122195 (2015).
35. Wang, D. *et al.* Peroxisome proliferator-activated receptor δ promotes colonic inflammation and tumor growth. *Proc. Natl Acad. Sci. USA* **111,** 7084–7089 (2014).
36. Wang, D. *et al.* Crosstalk between peroxisome proliferator-activated receptor δ and VEGF stimulates cancer progression. *Proc. Natl Acad. Sci. USA* **103,** 19069–19074 (2006).
37. Park, B. H., Vogelstein, B. & Kinzler, K. W. Genetic disruption of PPARδ decreases the tumorigenicity of human colon cancer cells. *Proc. Natl Acad. Sci. USA* **98,** 2598–2603 (2001).
38. Zuo, X. *et al.* Targeted genetic disruption of peroxisome proliferator-activated receptor-delta and colonic tumorigenesis. *J. Natl. Cancer Inst.* **101,** 762–767 (2009).
39. Gupta, R. A. *et al.* Activation of nuclear hormone receptor peroxisome proliferator-activated receptor-δ accelerates intestinal adenoma growth. *Nature Med.* **10,** 245–247 (2004).
40. Barak, Y. *et al.* Effects of peroxisome proliferator-activated receptor δ on placentation, adiposity, and colorectal cancer. *Proc. Natl Acad. Sci. USA* **99,** 303–308 (2002).

Supplementary Information is available in the online version of the paper.

Acknowledgements This work was supported by the Howard Hughes Medical Institute (S.H.O. and D.M.S.), Ellison Medical Foundation Aging grant (D.M.S.), NIH (R01 CA103866 and AI47389; D.M.S.), NIH (K08 CA198002; J.R.), Department of Defense PRCRP Career Development Award CA120198 (J.R.), NIH (R00 AG045144; Ö.H.Y.), NIH (R00 AG041765; D.W.L.), Center for the Study of Inflammatory Bowel Diseases from the Massachusetts General Hospital NIH (DK043351; Ö.H.Y.), NIH Cancer Center Support (core) grant P30-CA14051 (Ö.H.Y.), Kathy and Curt Marble Cancer Research Fund (Ö.H.Y.), American Federation of Aging Research (AFAR; Ö.H.Y.), and V Foundation Scholar grant (J.R. and Ö.H.Y.). M.D.M. is supported by a Koch MIT Ludwig Center post-doctoral fellowship, D.K. receives fellowship support from MGH (T32DK007191), and M.M.M. is a Robert Black Fellow of the Damon Runyon Cancer Research Foundation. We thank the Koch Institute Swanson Biotechnology Center (SBC) for technical support, specifically the Hope Babette Tang (1983) Histology Facility and Kathleen Cormier. We thank S. Holder for superior histology and help with special stains. We thank P. Wisniewski and G. Paradis of the Whitehead flow cytometry and Koch core facilities, respectively, for their expertise in cell sorting. We thank members of the Yilmaz laboratory for discussions.

Author Contributions Ö.H.Y., S.B., M.D.M. and J.R. performed all experiments, and participated in their design and interpretation. J.R. optimized the colonoscopy transplantation assay, with help from A.A., M.D.M. and Ö.H.Y. S.-J.H. performed the mRNA-sequencing and analysis, with help from G.W.B., S.B., L.P. and Y.K. K.E.B.-R., A.A. and M.D.M. performed and interpreted the immunohistochemistry and *in situ* hybridization, under the guidance of Ö.H.Y. S.B. performed the single-cell analysis, with assistance from M.E.X., R.D., G.G., G.-C.Y. and A.S. M.S. and G.P.N. performed electron microscopy and helped with its interpretation. S.S., V.D. and Ö.H.Y. performed all pathology on the mice with help from J.R., and participated in the design and interpretation of experiments. M.E.X., E.A., R.D., M.A.-R., M.M.M. and D.W.L. supplied HFD-fed mice and provided experimental support. C.R.F. and N.G. provided assistance with the acquisition of human samples, while D.K. performed and interpreted the human cell culture experiments. S.H.O. and D.M.S. participated in the design and interpretation of experiments. Ö.H.Y. wrote the paper with support from S.B., M.D.M. and J.R.

Author Information RNA-sequencing data have been deposited in the Gene Expression Omnibus (GEO) database under accession number GSE67324. Reprints and permissions information is available at www.nature.com/reprints. The authors declare no competing financial interests. Readers are welcome to comment on the online version of the paper. Correspondence and requests for materials should be addressed to D.M.S. (sabatini@wi.mit.edu) or Ö.H.Y. (ohyilmaz@mit.edu).

METHODS

Mice, HFD and drug treatment. Mice were housed in the Unit for Laboratory Animal Medicine at the Whitehead Institute for Biomedical Research and Koch Institute for Integrative Cancer Research. The following strains were obtained from the Jackson Laboratory: *Lgr5-EGFP-IRES-CreERT2* (strain name: B6.129P2-Lgr5$^{tm1(cre/ERT2)Cle}$/J, stock number 008875), *Rosa26-lacZ* (strain name: B6.129S4-Gt(ROSA)26Sor^{tm1Sor}/J, stock number 003474), *db/db* (strain name: B6.BKS(D)-Lepr^{jb}/J, stock number 000697), *Ppard*$^{L/L}$ (strain name: B6.129S4-Ppard^{tm1Rev}/J, stock number 005897). *Apc*$^{loxp\ exon\ 14}$ (*Apc*$^{L/L}$) has been previously described[41]. *Villin-CreERT2* was a gift from S. Robine. Long-term HFD was achieved by feeding male and female mice a dietary chow consisting of 60% kcal fat (Research Diets D12492) beginning at the age of 8–12 weeks and extending for a period of 9–14 months. Control mice were sex- and age-matched and fed standard chow *ad libitum*. GW501516 (Enzo) was reconstituted in DMSO at 4.5 mg ml^{-1} and diluted 1:10 in a solution of 5% PEG400 (Hampton Research), 5% Tween80 (Sigma), 90% H_2O for a daily intraperitoneal injection of 4 mg kg^{-1}. *Apc* exon 14 was excised by tamoxifen suspended in sunflower seed oil (Spectrum S1929) at a concentration of 10 mg ml^{-1} and 250 μl per 25 g of body weight, and administered by intraperitoneal injection twice over 4 days before collecting tissue. *Ppard*$^{L/L}$ mice were administered 4–5 intraperitoneal injections of tamoxifen on alternate days. Mice were analysed within 2 weeks of the last tamoxifen injection. BrdU was prepared at 10 mg ml^{-1} in PBS, passed through a 0.22-μm filter and injected at 100 mg kg^{-1}.

Immunohistochemistry and immunofluorescence. As previously described[1], tissues were fixed in 10% formalin, paraffin embedded and sectioned. Antigen retrieval was performed with Borg Decloaker RTU solution (Biocare Medical) in a pressurized Decloaking Chamber (Biocare Medical) for 3 min. Antibodies used: rat anti-BrdU (1:2,000 (immunohistochemistry (IHC)), 1:1,000 (immunofluorescence (IF)) Abcam 6326), rabbit chromogranin A (1:4,000 (IHC), 1:250 (IF), Abcam 15160), rabbit monoclonal non-phospho β-catenin (1:800 (IHC), 1:400 (IF), CST 8814S), mouse monoclonal β-catenin (1:200, BD Biosciences 610154), rabbit polyclonal lysozyme (1:250, Thermo RB-372-A1), rabbit polyclonal MUC2 (1:100, Santa Cruz Biotechnology 15334), rabbit monoclonal OLFM4 (1:10,000, gift from CST, clone PP7), Biotin-conjugated secondary donkey anti-rabbit or anti-rat antibodies were used from Jackson ImmunoResearch. The Vectastain Elite ABC immunoperoxidase detection kit (Vector Labs PK-6101) followed by Dako Liquid DAB+ Substrate (Dako) was used for visualization. For immunofluorescence, Alexa Fluor 568 secondary antibody (Invitrogen) was used with Prolong Gold (Life Technologies) mounting media. All antibody incubations involving tissue or sorted cells were performed with Common Antibody Diluent (Biogenex). Organoids were fixed with 4% paraformaldehyde, permabilized with 0.5% Triton X-100 in PBS, rinsed with 100 mM glycine in PBS, blocked with 10% donkey serum in PBS, incubated overnight with primary antibody at 4 °C, rinsed and incubated with Alexa Fluor 568 secondary antibody (Invitrogen), and mounted with Prolong Gold (Life Technologies) mounting media.

***In situ* hybridization.** The *in situ* hybridization probes used in this study correspond to expressed sequence tags or fully sequenced cDNAs obtained from Open Biosystems. The accession numbers (IMAGE mouse cDNA clone in parenthesis) for these probes are as follows: mouse *Olfm4* BC141127 (9055739), mouse *Crp4* BC134360 (40134597). Both sense and antisense probes were generated to ensure specificity by *in vitro* transcription using DIG RNA labelling mix (Roche) according to the manufacturer's instructions and to previously published detailed methods[23,42]. Single-molecule *in situ* hybridization was performed using Advanced Cell Diagnostics RNAscope 2.0 HD Detection Kit.

Radiation and clonogenic microcolony assay. Adult mice were exposed to 15 Gy of ionizing irradiation from a 137-caesium source (GammaCell) and euthanized after 72 h. The number of surviving crypts per length of the intestine was enumerated from haematoxylin-and-eosin-stained sections[15].

Immunopreciptation and immunoblotting. Antibodies: rabbit polyclonal anti-PPAR-δ (1:100, Thermo PA1-823A), rabbit polyclonal anti-CPT1a (1:250, ProteinTech 15184-1-AP), rabbit polyclonal anti-HMGCS2 (1:500, Sigma AV41562), rabbit monoclonal anti-FABP1 (1:1,000, Abcam ab129203), NF-κB Sampler Pathway Kit (CST, 9936S), mouse monoclonal anti-STAT-3 (CST, 9139P), rabbit monoclonal anti-P-STAT3 (Y705) XP (CST, 9145P), mouse monoclonal anti-CREB (CST, 86B10), mouse monoclonal anti-β-catenin (1:200, BD Biosciences 610154), rabbit polyclonal anti-γ-tubulin (1:1,000, Sigma T5192). For immunoprecipitation assays, crypts were collected and nuclear extraction was carried out using Abcam nuclear extraction kit (ab113474) following manufacturer's instructions. Nuclear extracts were incubated with 5 μg anti-PPAR-δ antibody (Thermo), or anti-rabbit IgG control antibody (Santa Cruz) overnight at 4 °C followed by 2 h of incubation with Dynabeads Protein G for immunoprecipitation. Protein complexes bound to antibody and beads were washed five times and eluted with Laemmli sample buffer. Samples were resolved by SDS–PAGE. Protein interaction was analysed by immunoblotting.

Lgr5-GFP^{hi} ISCs or Lgr5-GFP^{low} progenitors were sorted directly into Laemmli sample buffer and boiled for 5 min. Samples were resolved by SDS–PAGE and analysed by immunoblotting with horseradish peroxidase (HRP)-conjugated IgG secondary antibodies (1:10,000, Santa Cruz Biotechnology sc-2054) and Western Lightning Plus-ECL detection kit (Perkin Elmer NEL104001EA)

Flow cytometry and isolation of ISCs, colonic stem cells and Paneth cells. As previously reported and briefly summarized here, small intestines and colons were removed, washed with cold PBS without magnesium chloride and calcium (PBS−/−) opened longitudinally, and then cut into 3–5-mm fragments. Pieces were washed several times with cold PBS−/− until clean, washed 2–3 with PBS−/− EDTA (10 mM), incubated on ice for 90–120 min, and gently shook at 30-min intervals. Crypts were then mechanically separated from the connective tissue by more rigorous shaking, and then filtered through a 70-μm mesh into a 50-ml conical tube to remove villus material (for small intestine) and tissue fragments. Crypts were removed from this step for crypt culture experiments and embedded in Matrigel with crypt culture media. For ISC isolation, the crypt suspensions were dissociated to individual cells with TrypLE Express (Invitrogen). Cell labelling consisted of an antibody cocktail comprising CD45-PE (eBioscience, 30-F11), CD31-PE (Biolegend, Mec13.3), Ter119-PE (Biolegend, Ter119), CD24-Pacific Blue (Biolegend, M1/69), CD117-APC/Cy7 (Biolegend, 2BS), and EPCAM-APC (eBioscience, G8.8). ISCs were isolated as Lgr5-EGFP^{hi}Epcam^{+}CD24$^{low/-}$CD31^{-}Ter119^{-}CD45^{-}7-AAD^{-}. EGFP^{low} progenitors were isolated as EGFP^{low}Epcam^{+}CD24$^{low/-}$CD31^{-}Ter119^{-}CD45^{-}7-AAD^{-}, and Paneth cells from small intestine were isolated as CD24^{hi}Sidescatter^{hi}Lgr5-EGFP^{-}Epcam^{+}CD31^{-}Ter119^{-}CD45^{-}7-AAD^{-} with a BD FACS Aria II SORP cell sorter into supplemented crypt culture medium for culture. Dead cells were excluded from the analysis with the viability dye 7-AAD (Life Technologies). When indicated, populations were cytospun (Thermo Cytospin 4) at 800 r.p.m. for 2 min, or allowed to settle at 37 °C in fully humidified chambers containing 5% CO_2 onto poly-L-lysine-coated slides (Polysciences). The cells were subsequently fixed in 4% paraformaldehyde (pH 7.4, Electron Microscopy Sciences) before staining.

Culture media for crypts and isolated cells. Isolated crypts were counted and embedded in Matrigel (Corning 356231 growth factor reduced) at 5–10 crypts per μl and cultured in a modified form of medium as described previously[13]. Unless otherwise noted, Advanced DMEM (Gibco) was supplemented by EGF 40 ng ml^{-1} (R&D), Noggin 200 ng ml^{-1} (Peprotech), R-spondin 500 ng ml^{-1} (R&D or Sino Biological), *N*-acetyl-L-cysteine 1 μM (Sigma-Aldrich), N2 1X (Life Technologies), B27 1X (Life Technologies), Chiron 10 μM (Stemgent), Y-27632 dihydrochloride monohydrate 20 ng ml^{-1} (Sigma-Aldrich). Colonic crypts were cultured in 50% conditioned medium derived from L-WRN cells supplemented with Y-27632 dihydrochloride monohydrate 20 ng ml^{-1}, as described[43]. Approximately 25–30 μl droplets of Matrigel with crypts were plated onto a flat bottom 48-well plate (Corning 3548) and allowed to solidify for 20–30 min in a 37 °C incubator. Three hundred microlitres of crypt culture medium was then overlaid onto the Matrigel, changed every 3 days, and maintained at 37 °C in fully humidified chambers containing 5% CO_2. Clonogenicity (colony-forming efficiency) was calculated by plating 50–300 crypts and assessing organoid formation 3–7 days or as specified after initiation of cultures. Palmitic acid (Cayman Chemical Company 10006627 conjugated to BSA), oleic acid (Sigma O1008), lipid mixture (Sigma L0288), or GW501516 (Enzo) were added immediately to cultures at 30 μM (palmitic acid, oleic acid), 2% (lipid mixture), and 1 μM (GW501516). 4-OH tamoxifen (Calbiochem, 579002, 10 nM) was added to organoid cultures derived from *Ppard*$^{L/L}$; Villin-CreERT2 (*Ppard* IKO) crypts to ensure *Ppard* excision in the *ex vivo* fatty acid or GW501516 experiments.

Isolated ISCs or progenitor cells were centrifuged for 5 min at 250*g*, resuspended in the appropriate volume of crypt culture medium (500–1,000 cells μl^{-1}), then seeded onto 25–30 μl Matrigel (Corning 356231 growth factor reduced) containing 1 μM Jagged (Ana-Spec) in a flat bottom 48-well plate (Corning 3548). Alternatively, ISCs and Paneth cells were mixed after sorting in a 1:1 ratio, centrifuged, and then seeded onto Matrigel. The Matrigel and cells were allowed to solidify before adding 300 μl of crypt culture medium. The crypt media was changed every second or third day. Organoids were quantified on days 3, 7 and 10 of culture, unless otherwise specified.

Secondary mouse organoid assays. For secondary organoid assays, either individual primary organoids or many primary organoids were mechanically dissociated and then replated, or organoids were dissociated for 10 min in TrypLE Express at 32 °C, resuspended with SMEM (Life Technologies), centrifuged (5 min at 250*g*) and then resuspended in cold SMEM with the viability dye 7-AAD. Live cells were sorted and seeded onto Matrigel as previously described in standard crypt

media (not supplemented with lipids or GW501516). Secondary organoids were enumerated on day 4, unless otherwise specified.

Human crypt cultures. Human biopsies were obtained from patients with informed consent undergoing intestinal resection at the Massachusetts General Hospital (MGH). The MGH Institutional Review Board committee and Massachusetts Institute of Technology Committee on the Use of Humans as Experimental Subjects approved the study protocols. Crypts were isolated[43], embedded in Matrigel and subsequently exposed to lipid mixture, palmitic acid or GW501516 (as described in earlier). Cultures were passaged weekly and maintained for 3–4 weeks. To passage, equal numbers of organoids from each condition were disrupted with trypsin/EDTA. Numbers of organoids were counted 4–7 days after passaging into control media. Counts were normalized to numbers of organoids present in control wells and plotted. Statistical significance was calculated by performing analysis of variance (ANOVA) multiple comparisons of the means for each group. For quantitative RNA expression analysis, organoids were dissociated, cells were selected as a live population by flow cytometry (7-AAD, Life Technologies), and sorted into Tri Reagent (Life Technologies) for RNA isolation.

Electron microscopy. After 5 days of culturing, intestinal organoids were placed into Karnovsky's KII solution (2.5% glutaraldehyde, 2.0% paraformaldehyde, 0.025% calcium chloride, in a 0.1 M sodium cacodylate buffer, pH 7.4) and fixed overnight. Subsequently, they were post-fixed in 2.0% osmium tetroxide, stained en bloc with uranyl acetate, dehydrated in graded ethanol solutions, infiltrated with propylene oxide/Epon mixtures, flat embedded in pure Epon, and polymerized overnight at 60 °C. Then 1-μm sections were cut, stained with toluidine blue, and examined by light microscopy. Representative areas were chosen for electron microscopic study and the Epon blocks were trimmed accordingly. Thin sections were cut with an LKB 8801 ultramicrotome and diamond knife, stained with Sato's lead, and examined in a FEI Morgagni transmission electron microscope. Images were captured with an AMT (Advanced Microscopy Techiques) 2K digital CCD camera.

RNA isolation. For RNA sequencing (RNA-seq), total RNA was extracted from 200,000 sorted Lgr5-GFP^{hi} ISCs and Lgr5-GFP^{low} progenitors by pooling 2–5 71-week-old HFD male or control mice using Tri Reagent (Life Technologies) according to the manufacturer's instructions, except for an overnight isopropanol precipitation at −20 °C. From the total RNA, poly(A)$^+$ RNA was selected using Oligo(dT)$_{25}$-Dynabeads (Life technologies) according to the manufacturer's protocol.

RNA-seq library preparation. Strand-specific RNA-seq libraries were prepared using the dUTP-based, Illumina-compatible NEXTflex Directional RNA-Seq Kit (Bioo Scientific) according to the manufacturer's directions. All libraries were sequenced with an Illumina HiSeq 2000 sequencing machine.

Processing of RNA-seq reads and measuring expression level. For RNA-seq data analysis, raw stranded reads (40 nucleotides) were trimmed to remove adaptor and bases with quality scores below 20, and reads shorter than 35 nucleotides were excluded. High-quality reads were mapped to the mouse genome (mm10) with TopHat version 1.4.1 (ref. 44), using known splice junctions from Ensembl Release 70 and allowing at most two mismatches. Genes were quantified with htseq-count (with the 'intersect strict' mode) using Ensembl Release 70 gene models. Gene counts were normalized across all samples using estimateSizeFactors from the DESeq R/Bioconductor package[45]. Differential expression analysis was also performed between two samples of interest with DESeq. GSEA (http://software.broadinstitute.org/gsea/index.jsp) was performed by using the pre-ranked (according to their ratios) 8,240 differentially expressed genes as the expression data set. Motif Analysis was performed using Haystack motif enrichment tool: http://github.com/lucapinello/Haystack[46].

Single-cell gene expression analysis. In total, 24 single Lgr5-GFP^{hi} ISCs and 72 single Lgr5-GFP^{low} progenitor cells were sorted from control or HFD-fed mice ($n = 2$ mice per group) for single-cell gene expression analysis. For one-tube single-cell sequence-specific preamplification, individual primer sets of β-catenin target genes (total of 96, Supplementary Table 2) were pooled to a final concentration of 0.1 mM for each primer. Single cells were directly sorted into 96-well plates containing 5 μl RT–PCR master mix (2.5 μl CellsDirect reaction mix, Invitrogen; 0.5 μl primer pool; 0.1 μl reverse transcriptase/Taq enzyme, Invitrogen; 1.9 μl nuclease-free water) in each well. Immediately after, plates were placed on PCR machine for preamplification. Sequence-specific preamplification PCR protocol was as following: 60 min at 50 °C for cell lysis and sequence-specific reverse transcription; then 3 min at 95 °C for reverse transcriptase inactivation and Taq polymerase activation. cDNA was then amplified by 20 cycles of 15 s at 95 °C for initial denaturation, 15 min at 60 °C for annealing and elongation. After preamplificiation, samples were diluted 1:5 before high-throughput microfluidic real-time PCR analysis using Fluidigm platform. Amplified single-cell cDNA samples were assayed for gene expression using individual qRT–PCR primers and 96.96 dynamic arrays on a BioMark System by following manufacturers protocol (Fluidigm). To confirm PPAR-δ-mediated induction of the most upregulated genes ($n = 3$ mice, 24 ISCs and 72 progenitors per group), or for single-cell analysis of organoid composition ($n = 3$ mice, 48 cells per group) and *db/db* mice ($n = 3$, 48 cells per group) standard single-cell qRT–PCR was performed using preamplified cDNA with corresponding primers. For Fluidigm analysis, threshold cycle (C_t) values were calculated using the BioMark Real-Time PCR Analysis software (Fluidigm). See Supplementary Information for raw gene expression data. Gene expression levels were estimated by subtracting the C_t values from the background level of 35, which approximately represent the $\log_2$ gene expression levels. The t-Distributed stochastic neighbour embedding (t-SNE) analysis[47] was performed using the MATLAB toolbox for dimensionality reduction. Differential expression analysis was conducted using the two-sided Wilcoxon–Mann–Whitney rank sum test implemented in the R coin package (https://www.r-project.org). *P* values were adjusted for multiple testing[48] using the p.adjust function in R with method = 'fdr' option. Fold changes were calculated as the difference of median of $\log_2$ expression levels for the two cell populations. Split violin plots were generated using the vioplot package and the vioplot2 function in R (https://gist.github.com/mbjoseph/5852613). The heatmap for β-catenin target genes was generated with the MultiExperiment Viewer (MeV) program (http://www.tm4.org/mev.html) using the correlation-based distance and average linkage method as parameters of the unsupervised hierarchical clustering of genes. The heatmap for organoid composition was generated using MATLAB. The percentages of *Jag1*/*Jag2*-upregulated cells were calculated based on the number of single cells whose $\log_2$ expression was above 15.

qRT–PCR. Approximately 25,000 cells were sorted into Tri Reagent (Life Technologies) and total RNA was isolated according to the manufacturer's instructions with following modification: the aqueous phase containing total RNA was purified using the RNeasy plus kit (Qiagen). RNA was converted to cDNA with the cDNA synthesis kit (Bio-Rad). qRT–PCR was performed with diluted cDNA (1:5) in three wells for each primer and SYBR green master mix (Bio-Rad) on Bio-Rad iCycler RT–PCR detection system. For organoid experiments, 1,000 live cells were sorted and qRT–PCR optimized for low cell numbers (<1,000) was performed after sequence specific pre-amplification (cDNA diluted 1:200 in three wells for each primer) as described in single-cell gene expression analysis. All qRT–PCR experiments were repeated at least three independent times. Primers used are listed on Supplementary Table 1.

Orthotopic transplantation. *Apc*$^{L/L}$; *Lgr5-EGFP-IRES-CreERT2* mice were treated with vehicle or GW501516 for 1 month, and then injected with two intraperitoneal doses of tamoxifen. Four days later, *Apc*-null Lgr5-GFP^{hi} ISCs and Lgr5-GFP^{low} progenitors were sorted by flow cytometry, as described earlier. For primary cell transplantations, 10,000 *Apc*-null Lgr5-GFP^{hi} ISCs and Lgr5-GFP^{low} progenitors were resuspended into 90% crypt culture media (as described) and 10% Matrigel, then transplanted into the colonic lamina propria of C57BL/6 recipient mice by optical colonoscopy using a custom injection needle (Hamilton Inc., 33-gauge, small Hub RN NDL, 16 inches long, point 4, 45 degree bevel, like part number 7803-05), syringe (Hamilton Inc. part number 7656-01), and transfer needle (Hamilton Inc. part number 7770-02). Optical colonoscopy was performed using a Karl Storz Image 1 HD Camera System, Image 1 HUB CCU, 175 Watt Xenon Light Source, and Richard Wolf 1.9mm/9.5 Fr Integrated Telescope (part number 8626.431). Four injections were performed per mouse. Mice then underwent colonoscopy 8 weeks later to assess tumour formation. Colonoscopy videos and images were saved for offline analysis. Following sacrifice, the distal colons were excised and fixed in 10% formalin, then examined by haematoxylin and eosin section to identify adenomas. Histology images were reviewed by gastrointestinal pathologists who were blinded to the treatment groups (S.S., V.D. and Ö.H.Y.).

Statistics and animal models. All experiments reported in Figs 1–5 were repeated at least three independent times, except for Figs 3a, 4c, d, which were repeated twice. All samples represent biological replicates. For mouse organoid assays, 2–4 wells per group with at least 3 different mice were analysed. For human organoid assays, 4 wells per group with 4 different patient samples were analysed and experiments were repeated 4 times. All centre values shown in graphs refer to the mean. For statistical significance of the differences between the means of two groups, we used two-tailed Student's *t*-tests. Statistical significance in Fig. 3k was calculated by performing ANOVA multiple comparisons of the means for each group. No samples or animals were excluded from analysis, and sample size estimates were not used. Animals were randomly assigned to groups. Studies were not conducted blinded, with the exception of all histological analyses and Fig. 5c, h. All experiments involving mice were carried out with approval from the Committee for Animal Care at MIT and under supervision of the Department of Comparative Medicine at MIT.

41. Colnot, S. *et al.* Colorectal cancers in a new mouse model of familial adenomatous polyposis: influence of genetic and environmental modifiers. *Lab. Invest.* **84,** 1619–1630 (2004).
42. Gregorieff, A. & Clevers, H. *In situ* hybridization to identify gut stem cells. *Curr. Protoc. Stem Cell Biol.* **Chapter 2,** Unit 2F.1 (2010).
43. Miyoshi, H. & Stappenbeck, T. S. *In vitro* expansion and genetic modification of gastrointestinal stem cells in spheroid culture. *Nature Protocols* **8,** 2471–2482 (2013).
44. Trapnell, C., Pachter, L. & Salzberg, S. L. TopHat: discovering splice junctions with RNA-Seq. *Bioinformatics* **25,** 1105–1111 (2009).
45. Anders, S. & Huber, W. Differential expression analysis for sequence count data. *Genome Biol.* **11,** R106 (2010).
46. Pinello, L., Xu, J., Orkin, S. H. & Yuan, G. C. Analysis of chromatin-state plasticity identifies cell-type-specific regulators of H3K27me3 patterns. *Proc. Natl Acad. Sci. USA* **111,** E344–E353 (2014).
47. van der Maaten, L. & Hinton, G. Visualizing Data using t-SNE. *J. Mach. Learn. Res.* **9,** 2579–2605 (2008).
48. Benjamini, Y. & Hochberg, Y. Controlling the false discovery rate – a practical and powerful approach to multiple testing. *J. Roy. Stat. Soc. B* **57,** 289–300 (1995).

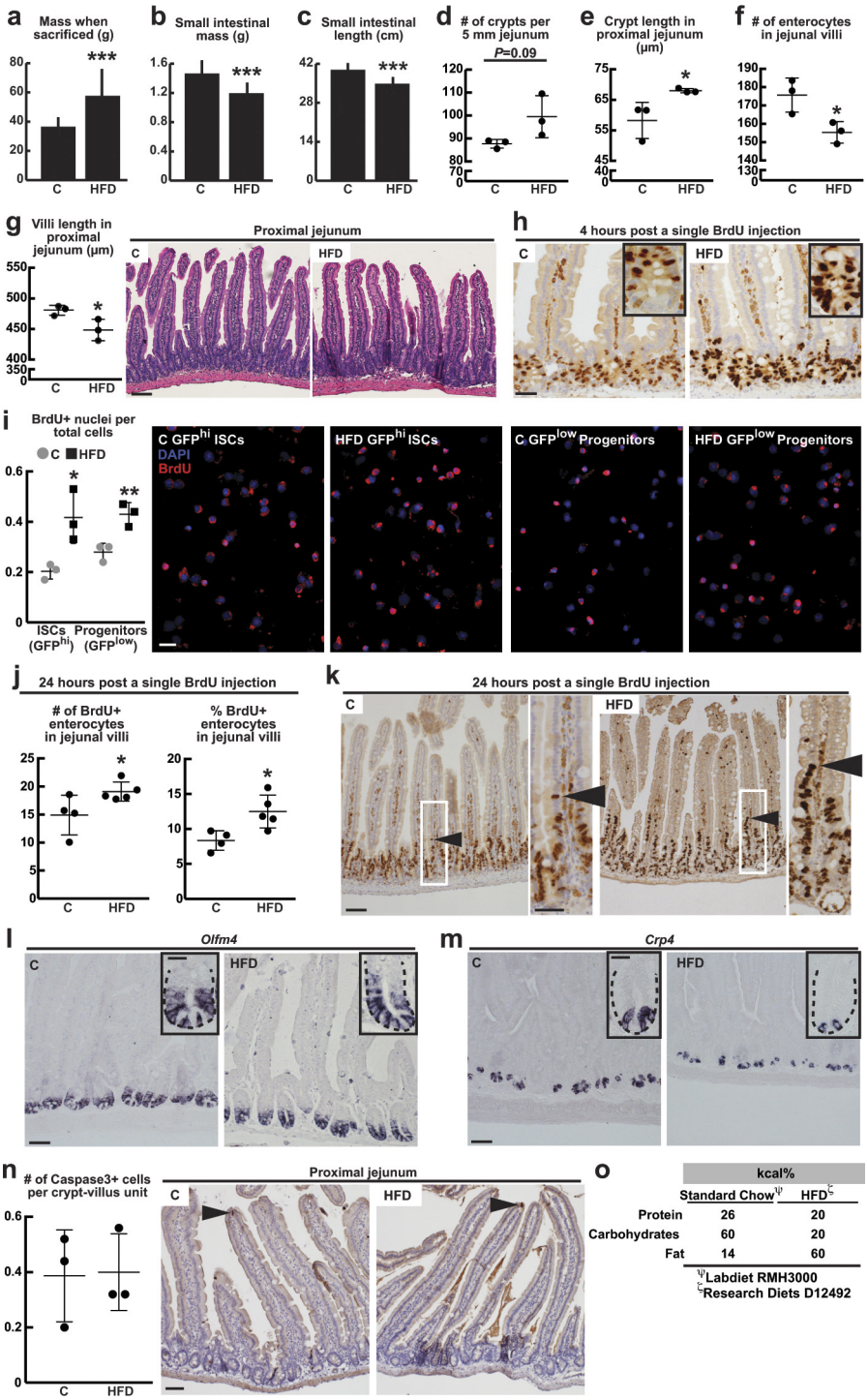

Extended Data Figure 1 | A HFD alters intestinal morphology and enhances intestinal progenitor proliferation. a–**g**, In comparison to mice fed a standard chow, mice on a HFD gained on average 50% mass (**a**, control: $n = 11$, HFD: $n = 15$), had reduced small intestinal mass and length (**b**, **c**, control: $n = 11$, HFD: $n = 15$), longer crypts and shorter villi (**e**, **g**, $n = 3$ each), and fewer villus enterocytes (**f**, $n = 3$). HFD did not change the density of crypts (**d**, $n = 3$) in the proximal jejunum. The proximal jejunum was defined as the length between 6 and 9 cm as measured from the pylorus (the distal portion of the stomach). **h**–**k**, HFD enhanced BrdU incorporation in ISCs (or crypt base columnar cells) and progenitor cells (or transit-amplifying cells) in the proximal jejunum (**h**, $n = 6$) and sorted cell populations (**i**, $n = 3$) after a 4-h pulse. HFD increased the total (**j**, control: $n = 4$, HFD: $n = 5$) and normalized numbers of BrdU-labelled enterocytes compared to controls after a 24-h pulse. Arrowhead (**k**) marks the leading edge of migrating BrdU-positive enterocyte. **l**, **m**, Representative images of *Olfm4* (**l**, $n = 3$) and *Crp4* (**m**, $n = 6$) *in situ* hybridizations from control and HFD-fed mice. **n**, No significant difference in the number of jejunal caspase3$^+$ cells was detected by immunohistochemistry. Images are representative of three separate experiments ($n = 3$); arrowheads indicate representative caspase3$^+$ enterocytes. **o**, The HFD chow (Research Diets D12492) provides a higher percentage of kilocalories from fat and conversely a lower percentage of kilocalories from protein and carbohydrates compared to a standard chow diet (Labdiet RMH3000). Unless otherwise indicated, data are mean ± s.d. from n independent experiments; $^*P < 0.05$, $^{**}P < 0.01$, $^{***}P < 0.001$ (Student's t-tests). Scale bars, 100 μm (**g**, **k**, **n**), 50 μm (**h**, **i**, **k** (inset), **l**, **m**) and 20 μm (**l**, **m**, insets); two separate fields of jejunum (**d**), and at least 15 crypts (**e**), 15 villi (**f**), 10 villi (**g**), 100 cells (**i**), 25 villi (**j**) and 25 crypt–villus units (**n**) were counted per sample in each independent experiment.

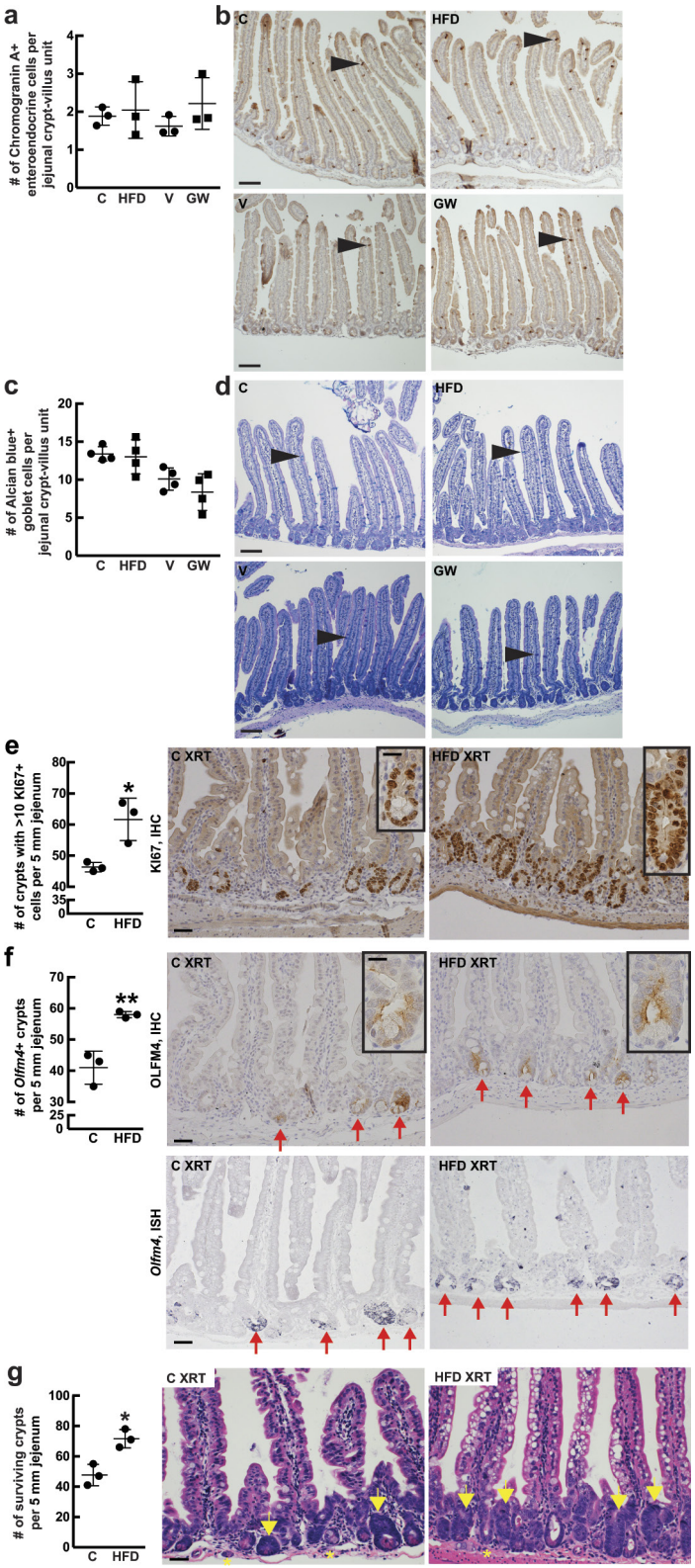

Extended Data Figure 2 | A HFD and PPAR-δ signalling have minimal effects on enteroendocrine and goblet cell differentiation but promote intestinal regeneration after 15 Gy irradiation. **a**, **b**, Quantification (**a**, $n = 3$) of immunostains (**b**, $n = 3$) for chromogranin A revealed no difference in the numbers of jejunal enteroendocrine cells (arrowheads) per crypt–villus unit in HFD-fed mice and GW501516-treated mice compared to their respective controls. **c**, **d**, Quantification (**c**, $n = 4$) of Alcian blue/PAS staining (**d**, $n = 4$) showed no difference in mucinous goblet cells (arrowhead) in HFD-fed and GW501516-treated mice compared to their respective controls. **e**, **f**, A HFD increased the number of regenerating crypts as measured by an increased number of crypts containing at least ten Ki67$^+$ (a marker of proliferation) cells (**e**, $n = 3$) or at least one *Olfm4*$^+$ cell (**f**, $n = 3$) per 5 mm of jejunum by immunohistochemistry (IHC) or *in situ* hybridization (ISH). Arrows indicate *Olfm4*$^+$ crypts. **g**, Surviving crypt numbers after ionizing irradiation-induced (XRT) damage. Arrows denote regenerating crypts; asterisks denote aborted crypts ($n = 3$). Unless otherwise indicated, data are mean ± s.d. from *n* independent experiments. Scale bars, 100 μm (**b**, **d**), 50 μm (**e**–**g**) and 20 μm (**e**, **f**, insets); 50 crypt–villus units per sample were analysed (**a**, **c**) and approximately 50 crypts (**e**–**g**) were counted per sample in each independent experiment.

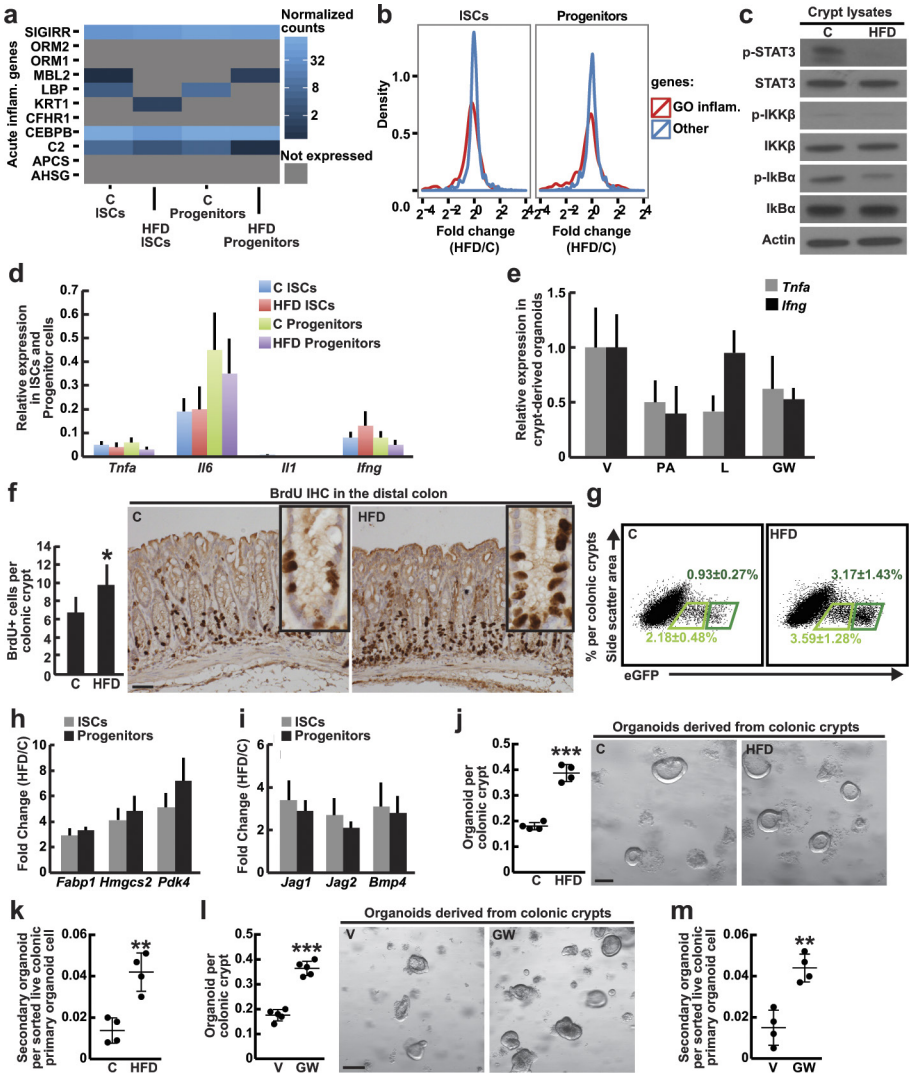

Extended Data Figure 3 | A HFD and fatty acids do not activate inflammatory pathways in intestinal crypts and organoids, while HFD and enforced PPAR-δ signalling enhance colonic stem-cell function. a, A HFD did not alter the normalized expression levels of inflammatory genes from the GSEA Molecular Signature Database (MSigDB; signature M6557) data set in ISCs and progenitors. **b**, A HFD did not induce differential expression of 'inflammatory response' genes from Gene Ontology (GO; 0006954) in ISCs (Lgr5-GFP^{hi}) or progenitors (Lgr5-GFP^{low}) compared to control. Fold changes of GO inflammatory response genes are indicated in red, and fold changes for all other genes are indicated in blue. **c**, HFD did not activate the NF-κB or the STAT-3 pathways in the intestinal crypt. Total and phosphorylated protein levels in crypt lysates were assessed by immunoblots ($n = 3$). For western blot source data, see Supplementary Fig. 1. **d**, A HFD did not induce pro-inflammatory gene expression in ISCs (Lgr5-GFP^{hi}) or progenitors (Lgr5-GFP^{low}). Relative expression levels compared to *Actb* were measured by qRT–PCR ($n = 5$). **e**, *Ex vivo* palmitic acid, lipid mixture or GW501516 treatment did not induce inflammatory gene expression in crypt-derived organoids compared to vehicle. Relative expression levels compared to *Actb* were assessed by qRT–PCR ($n = 4$, 12 wells per sample were analysed). **f**, A HFD boosted the number of BrdU-labelled cells as measured in distal colonic crypts compared to control (control $n = 6$, HFD $n = 5$) after a 4-h pulse. **g**, A HFD increased the frequency of colonic ISCs (Lgr5-GFP^{hi}, dark green) and progenitor cells (Lgr5-GFP^{low}, light green) ($n = 8$). **h**, **i**, A HFD enhanced PPAR-δ (**h**) and β-catenin (**i**) target gene expression in colonic ISCs and progenitors. Relative expression levels compared to *Actb* were determined by qRT–PCR ($n = 5$, all fold changes are significant with $P < 0.05$). **j**–**m**, Colonic crypts derived from HFD-fed (**j**, $n = 4$; **k**, $n = 4$) and GW501516-treated (**l**, $n = 5$; **m**, $n = 4$) mice demonstrated greater primary and secondary organoid-forming capacity compared to their respective controls. Representative images: day-4 organoids. Unless otherwise indicated, data are mean ± s.d. from n independent experiments; $^*P < 0.05$, $^{**}P < 0.01$, $^{***}P < 0.001$ (Student's t-tests). Scale bars, 50 μm (**f**), 100 μm (**j**) and 200 μm (**l**); 50 crypts per sample were analysed (**f**) in each independent experiment.

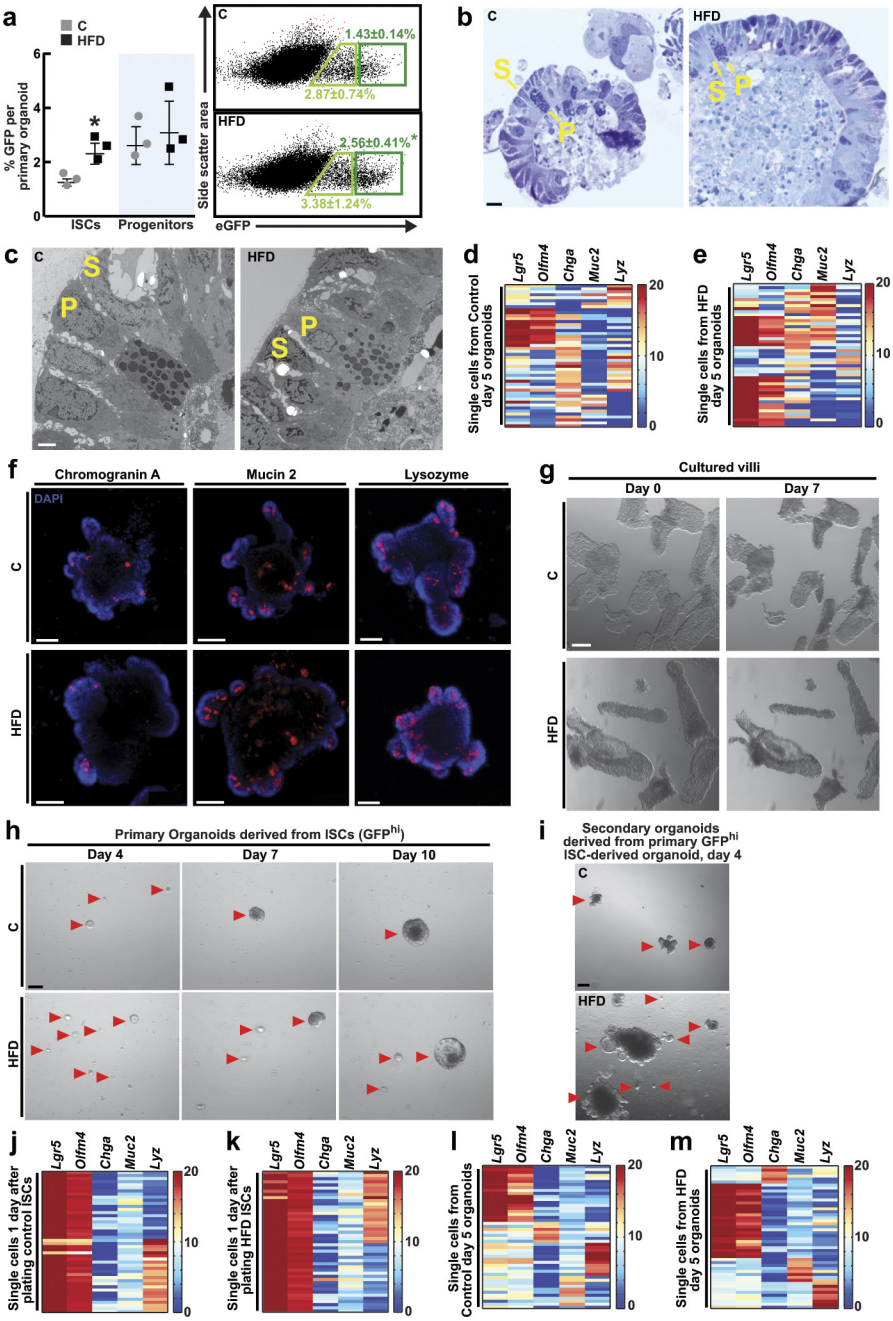

Extended Data Figure 4 | Characterization of HFD crypt and ISC-derived organoids. a, HFD organoids contained higher frequencies of ISCs (Lgr5-GFP^{hi}) compared to control ($n = 3$). **b**, **c**, Control and HFD organoids demonstrated no differences in morphologic ultrastructure as seen in 1-μm sections of control (left) and HFD (right) organoids counterstained with Toluidine Blue (**b**), and electron microscopy images of representative control (left) and HFD (right) organoids (**c**) ($n = 3$). **d**, **e**, Composition of organoids derived from control (**d**) and HFD (**e**) crypts as assessed by single-cell gene expression analysis. Organoids on day 5 contained ISCs (*Lgr5* and *Olfm4*), Paneth cells (*Lyz*), enteroendocrine cells (*Chga*), and goblet cells (*Muc2*). Forty-eight live cells per group were sorted and single-cell gene expression analysis was performed after pre-amplification using corresponding stem-cell and lineage primers (see Methods). **f**, Crypt-derived organoids from control or HFD-fed mice included chromogranin A-, mucin 2- and lysozyme-positive cells as assessed by immunofluorescence (blue = DAPI, red = cell-specific antibody). Images represent two experiments ($n = 2$). **g**, Cultured villi from control and HFD-fed mice lack the ability to form organoids. Images represent two experiments with 6 wells per sample ($n = 2$). **h**, ISCs from HFD-fed mice contained greater organoid-forming potential compared to controls. Arrowheads indicate representative organoids at days 4, 7 and 10 of culture ($n = 4$). **i**, Individually dissociated HFD primary organoids that were derived from single ISCs possessed more secondary organoid-forming ability than those from controls. ($n = 4$). Representative images: day-4 secondary organoids. **j**, **k**, Single-cell gene expression analysis revealed that ISCs from both control (**j**) and HFD (**k**) mice can beget Paneth cells (*Lyz*) within 24 h in culture (48 cells per group, see Methods). **l**, **m**, Composition of organoids derived from control (**l**) and HFD (**m**) ISCs (Lgr5-GFP^{hi}) as assessed by single-cell gene expression analysis (48 cells per group, see Methods). Organoids on day 5 contained ISCs (*Lgr5* and *Olfm4*), Paneth cells (*Lyz*), endocrine cells (*Chga*) and goblet cells (*Muc2*). Unless otherwise indicated, data are mean ± s.d. from *n* independent experiments; $^*P < 0.05$ (Student's *t*-tests). Scale bars, 20 μm (**b**), 2 μm (**c**), 50 μm (**f**), 200 μm (**g**, **i**) and 100 μm (**h**).

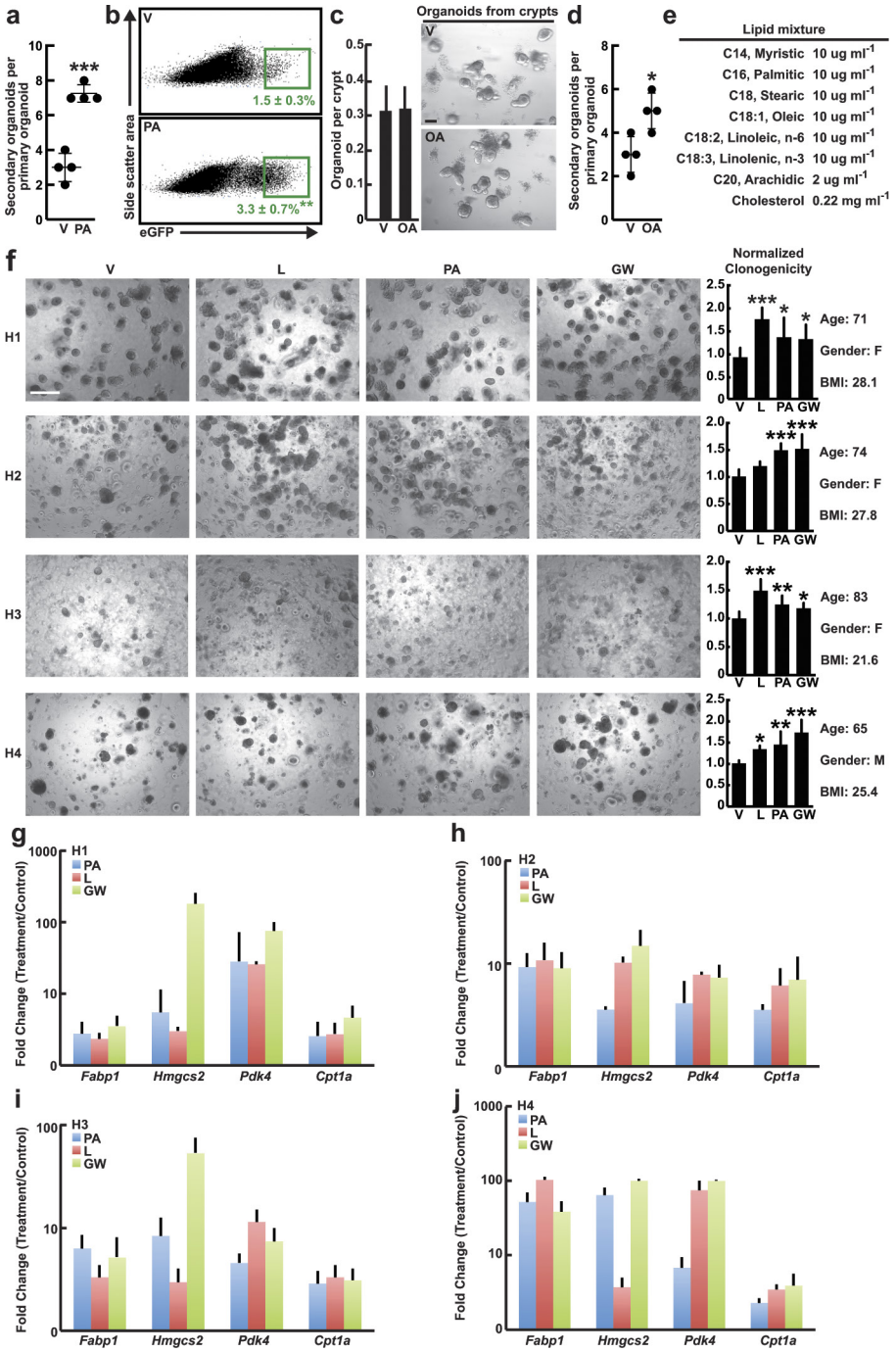

Extended Data Figure 5 | *Ex vivo* exposure of mouse and human organoids to fatty acids recapitulates aspects of a HFD.
a, **b**, Individually dissociated primary organoids possessed more secondary organoid-forming activity (**a**, $n = 4$, the mean number of secondary organoids subcloned from each of 5 primary organoids in 4 independent experiments), and contained a higher frequency of Lgr5-GFP^{hi} ISCs (**b**, $n = 3$) after 4 weeks of treatment with 30 μM palmitic acid compared to vehicle. **c**, Exposure of naive crypts to 30 μM oleic acid had no effect on primary organoid formation measured at day 7 ($n = 6$). Representative images: day-7 organoids. **d**, Individually dissociated primary organoids possessed more secondary-organoid-forming capacity after 4 weeks of treatment with 30 μM oleic acid ($n = 4$, the mean number of secondary organoids subcloned from each of 5 primary organoids in 4 independent experiments) compared to vehicle (same vehicle cohort used in **a** and **d**). **e**, Lipid mixture composition (Sigma L0288) as described by the manufacturer. **f**, *Ex vivo* treatment of human-derived small intestinal crypts (H1–H4) passaged in the presence of lipid mixture, palmitic acid or GW501516 augmented relative clonogenicity compared to vehicle, as shown in representative images from 4 independent experiments. H1: $n = 10$ (vehicle, palmitic acid, GW501516) and $n = 6$ (lipid mixture) wells were analysed. H2: $n = 16$ (vehicle), $n = 6$ (lipid), $n = 12$ (palmitic acid) and $n = 14$ (GW501516) wells were analysed. H3: $n = 10$ (vehicle), $n = 12$ (lipid, palmitic acid) and $n = 8$ (GW501516) wells were analysed. H4: $n = 7$ (vehicle, GW501516), $n = 6$ (lipid) and $n = 9$ (palmitic acid) wells were analysed. Age, gender and BMI are specified. **g**–**j**, Human crypt-derived organoids after *ex vivo* treatment with palmitic acid, lipid or GW501516 induced PPAR-δ target gene expression as assessed in passaged cultures with qRT–PCR ($n = 4$, 12 wells per sample were analysed, all fold changes are significant, $P < 0.05$). Unless otherwise indicated, data are mean ± s.d. from *n* independent experiments; $^*P < 0.05$, $^{**}P < 0.01$, $^{***}P < 0.001$ (Student's *t*-tests). Scale bars, 100 μm (**c**) and 500 μm (**f**).

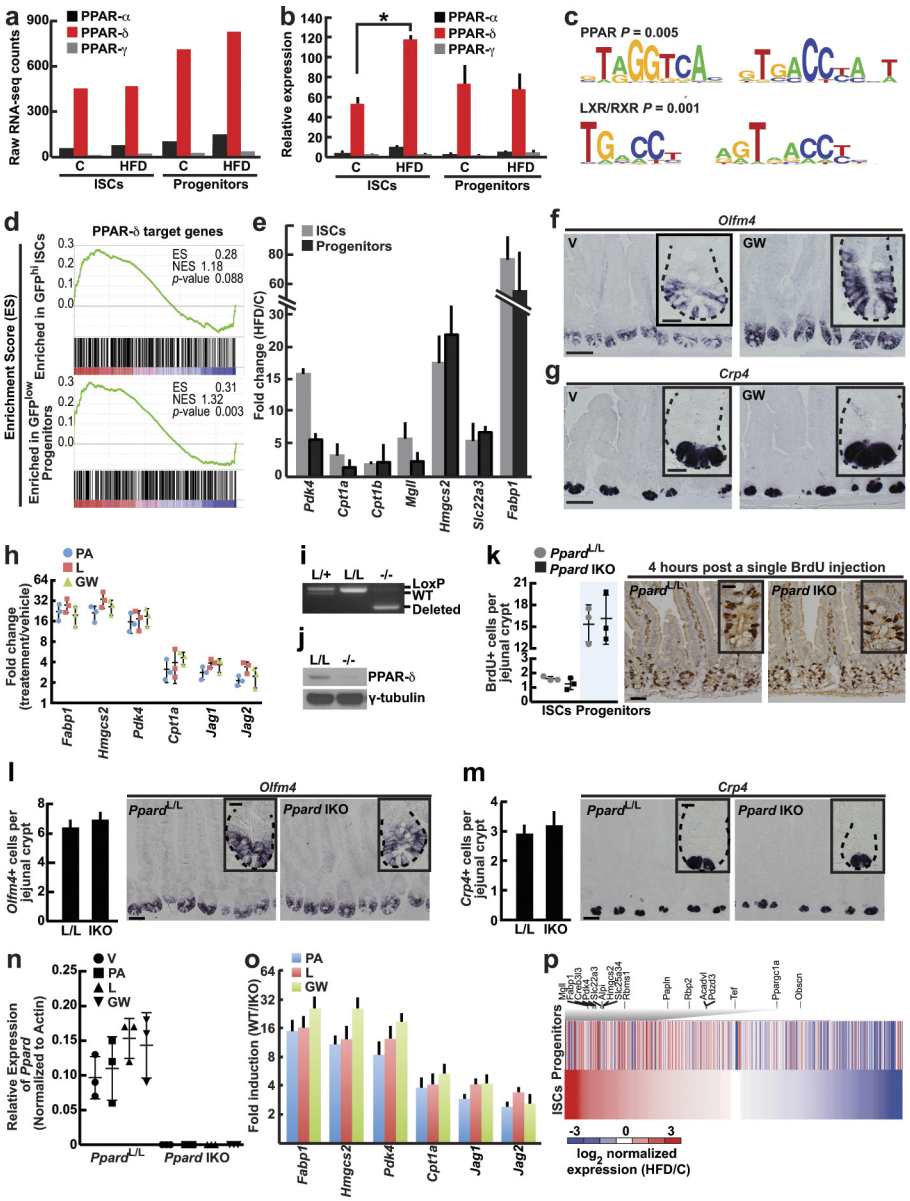

Extended Data Figure 6 | PPAR-δ is the predominant PPAR family member expressed in intestinal progenitors and mediates the effects of HFD. **a**, PPAR-δ is the most abundant PPAR family member in ISCs (Lgr5-GFP^{hi}) and progenitors (Lgr5-GFP^{low}) based on RNA-seq data. **b**, Confirmation of PPAR family member mRNA expression levels in ISCs (Lgr5-GFP^{hi}) and progenitors (Lgr5-GFP^{low}) by qRT–PCR ($n = 5$). **c**, Genes upregulated in HFD ISCs (Lgr5-GFP^{hi}) versus control ISCs were enriched in PPAR and LXR/RXR motifs. **d**, GSEA of RNA-seq data identified enrichment of PPAR-δ targets in ISCs (Lgr5-GFP^{hi}) and progenitors (Lgr5-GFP^{low}) with a HFD. **e**, Confirmation of induced PPAR-δ target gene expression in flow-sorted ISCs (Lgr5-GFP^{hi}) and progenitors (Lgr5-GFP^{low}) by qRT–PCR ($n = 5$). All fold changes were significant, $P < 0.05$. **f**, **g**, Representative images of *Olfm4*$^{+}$ (ISCs, **f**) and *Crp4*$^{+}$ (Paneth cells, **g**) *in situ* hybridization from vehicle and GW501516-treated mice (**f**, $n = 3$; **g**, $n = 4$). **h**, *Ex vivo* exposure of organoids to palmitic acid, lipid mixture or GW501516 stimulated PPAR-δ and β-catenin target gene expression ($n = 3$, all fold changes were significant, $P < 0.05$). **i**, **j**, Injection with tamoxifen (4 injections on alternating days) in *Ppard*$^{L/L}$; *Villin-CreERT2* mice led to efficient intestinal deletion (IKO) of *Ppard* (7 days after the last tamoxifen dose), as assessed by allele-specific deletion PCR (**i**, $n = 3$) and immunoblot analysis (**j**, $n = 3$) of crypts. For western blot source data, see Supplementary Fig. 1. **k**, Acute disruption of *Ppard* (8 days after the last tamoxifen dose) did not perturb ISC and progenitor proliferation, as determined 4-h after BrdU administration ($n = 3$). **l**, **m**, Acute *Ppard* deletion (8 days after the last tamoxifen dose) did not significantly alter *Olfm4*$^{+}$ ISCs numbers (L/L: $n = 5$, IKO: $n = 4$) (**l**) or *Crp4*$^{+}$ Paneth cell ($n = 5$) (**m**) numbers, as assessed by *in situ* hybridization. **n**, Loss of *Ppard* transcripts in *Ppard* IKO organoids was confirmed by qRT–PCR using deletion-specific primers ($n = 3$). **o**, PPAR-δ is required for the induction of PPAR-δ and β-catenin target gene expression in secondary organoids after *ex vivo* palmitic acid, lipid or GW501516 treatment ($n = 5$, all fold changes are significant, $P < 0.05$). **p**, Heat map of differentially expressed genes illustrated induction of a PPAR-δ program in HFD-derived ISCs and progenitors relative to controls. Unless otherwise indicated, data are mean ± s.d. from n independent experiments; *$P < 0.05$ (Student's t-tests). Scale bars, 50 μm (**f**, **g**, **k**–**m**) and 20 μm (insets); 50 crypts per sample were analysed in each independent experiment (**f**, **g**, **k**–**m**).

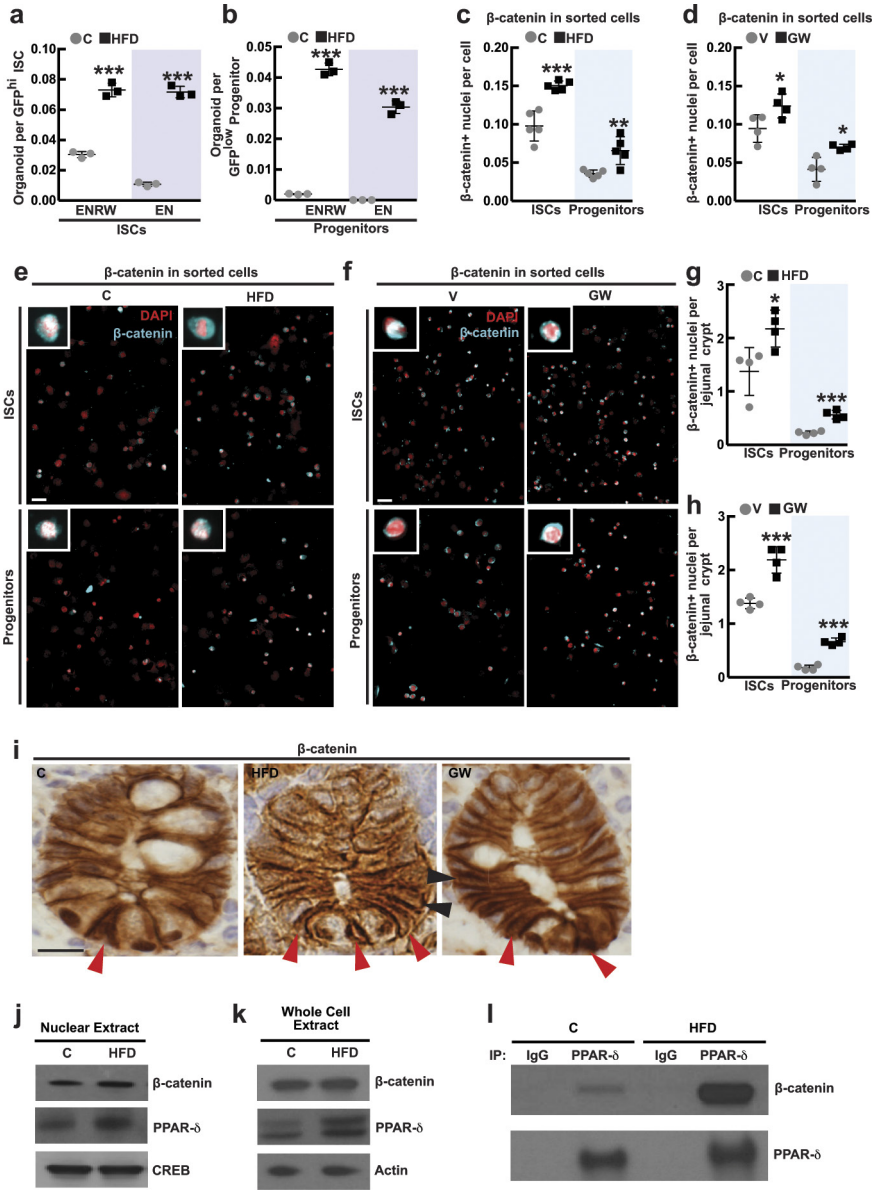

Extended Data Figure 7 | HFD and PPAR-δ signalling boost nuclear β-catenin localization and activity in intestinal progenitors. a, **b**, HFD-derived ISCs (**a**, Lgr5-GFP^{hi}) and progenitors (**b**, Lgr5-GFP^{low}) required less Wnt3a and R-spondin to initiate organoids than control ISCs, as measured by comparing organoid-formation in complete ENRW media, which includes EGF, Noggin, R-spondin and Wnt3a, versus EN media, which includes EGF and Noggin but lacks Wnt3a and R-spondin ($n = 3$). Control-derived progenitors, in contrast to HFD-derived progenitors, rarely formed organoids in either ENRW or EN media. **c**–**f**, HFD increased nuclear β-catenin localization in flow-sorted ISCs and progenitors from HFD (**c**, $n = 5$) and GW501516-treated (**d**, $n = 4$) mice as determined by immunofluorescence (red, DAPI; cyan, non-phosphorylated β-catenin, CST 8814S). At least 100 cells per sample were quantified. Representative images are shown in **e** and **f**. **g**–**i**, HFD (**g**) and GW501516 (**h**) treatment increased the numbers of ISCs and progenitors with β-catenin^{+} nuclei, as assessed by immunostaining ($n = 4$ each). Representative images are shown in **i**; arrowheads indicate representative nuclear β-catenin in ISCs (red) and progenitors (black). **j**–**l**, Association of PPAR-δ and β-catenin in control and HFD-derived intestinal crypts as shown by immunoprecipitation (IP) ($n = 3$). For western blot source data, see Supplementary Fig. 1. Unless otherwise indicated, data are mean ± s.d. from n independent experiments; $^{*}P < 0.05$, $^{**}P < 0.01$, $^{***}P < 0.001$ (Student's t-tests). Scale bars, 50 μm (**e**, **f**) and 20 μm (**i**); organoid assays: 2–4 wells per sample analysed (**a**, **b**), 50 crypts per sample were analysed in each independent experiment (**g**, **h**).

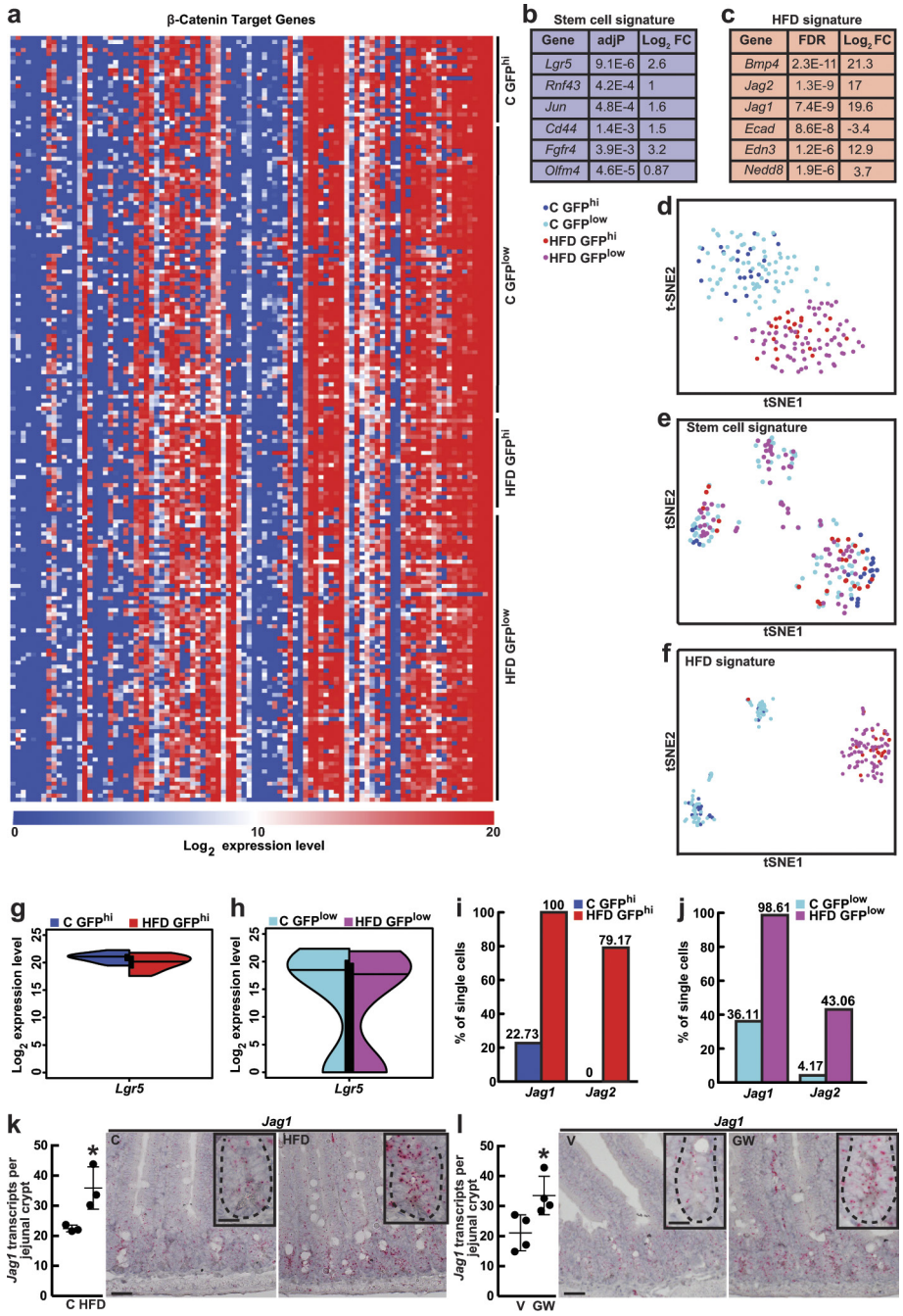

Gene	adjP	Log$_2$ FC
Lgr5	9.1E-6	2.6
Rnf43	4.2E-4	1
Jun	4.8E-4	1.6
Cd44	1.4E-3	1.5
Fgfr4	3.9E-3	3.2
Olfm4	4.6E-5	0.87

Gene	FDR	Log$_2$ FC
Bmp4	2.3E-11	21.3
Jag2	1.3E-9	17
Jag1	7.4E-9	19.6
Ecad	8.6E-8	-3.4
Edn3	1.2E-6	12.9
Nedd8	1.9E-6	3.7

Extended Data Figure 8 | HFD-mediated alterations in β-catenin target gene expression in single ISCs and progenitors. a, Heat map representation of β-catenin target gene expression in single ISCs (Lgr5-GFP^{hi}, 24 cells) and progenitors (Lgr5-GFP^{low}, 72 cells) (see Methods). **b**, Stem-cell signature genes were identified by comparing target gene expression in control ISCs (Lgr5-GFP^{hi}) to control progenitors (Lgr5-GFP^{low}). **c**, HFD signature genes were identified by comparing target gene expression in HFD ISCs to control ISCs (Lgr5-GFP^{hi}). **d**, t-Distributed stochastic neighbour embedding (tSNE) analysis of single cells using all β-catenin target genes. **e**, tSNE analysis of single cells using stem-cell signature genes. **f**, tSNE analysis of single cells using HFD signature genes. **g**, **h**, *Lgr5* expression was similar in HFD ISCs (Lgr5-GFP^{hi}) (**g**) and progenitors (Lgr5-GFP^{low}) (**h**) as compared to their respective controls. **i**, **j**, HFD increased the percentage of ISCs (Lgr5-GFP^{hi}) (**i**) and progenitors (Lgr5-GFP^{low}) (**j**), with increased *Jag1* and *Jag2* expression compared to their respective controls. **k**, **l**, HFD (**k**, $n = 3$) and GW501516 treatment (**l**, $n = 4$) augmented *Jag1* expression compared to control and vehicle treatments, respectively, as assayed by single-molecule *in situ* hybridization: *Jag1* is broadly expressed throughout the crypt. Unless otherwise indicated, data are mean ± s.d. from n independent experiments; $^*P < 0.05$ (Student's t-tests). Scale bars, 50 μm (**k**, **l**) and 20 μm (insets); more than 50 crypts per sample were analysed in each independent experiment (**k**, **l**). See Supplementary Information for raw gene expression data.

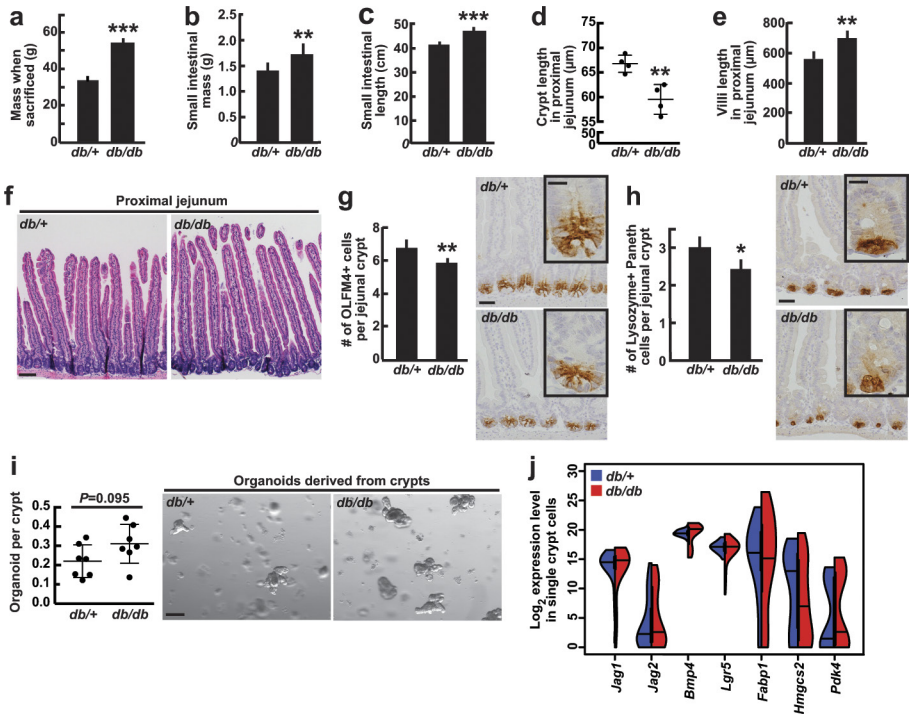

Extended Data Figure 9 | Characterization of obese *db/db* mouse intestines. a–f, At 4–5 months of age, homozygous *db/db* mice gained on average 50% more mass (**a**, $n = 9$), had increased small intestinal mass and length (**b**, **c**, $n = 9$), shallower crypts (**d**, $n = 4$) and longer villi (**e**, **f**, $n = 5$) than control *db/+* mice. **g**, **h**, Immunostains for OLFM4 ($n = 6$) and lysozyme ($n = 6$) revealed a slight reduction in the number of Olfm4^{+} ISCs and Paneth cells, respectively, in *db/db* mice compared to *db/+* controls. **i**, Organoid-forming capacity of *db/db* crypts was higher ($P = 0.095$) than *db/+* controls ($n = 7$). **j**, Single-cell gene expression analysis revealed no induction of PPAR-δ or β-catenin target gene expression in live, enriched stem and progenitor cells that are depleted of secretory cells (7-AAD^{-}Epcam^{+}CD24^{-}c-kit^{-} cells, 48 cells per group; see Methods) from *db/db* intestines compared to control intestines. Unless otherwise indicated, data are mean ± s.d. from *n* independent experiments; $^{*}P < 0.05$, $^{**}P < 0.01$, $^{***}P < 0.001$ (Student's *t*-tests). Scale bars, 100 μm (**f**), 50 μm (**g**, **h**), 20 μm (**g**, **h**, insets) and 200 μm (**i**); and at least 30 crypts (**d**), 20 villi (**e**) and 100 crypts (**g**, **h**) were assessed per sample in each independent experiment. All *db/db* and *db/+* mice were fed a standard chow diet.

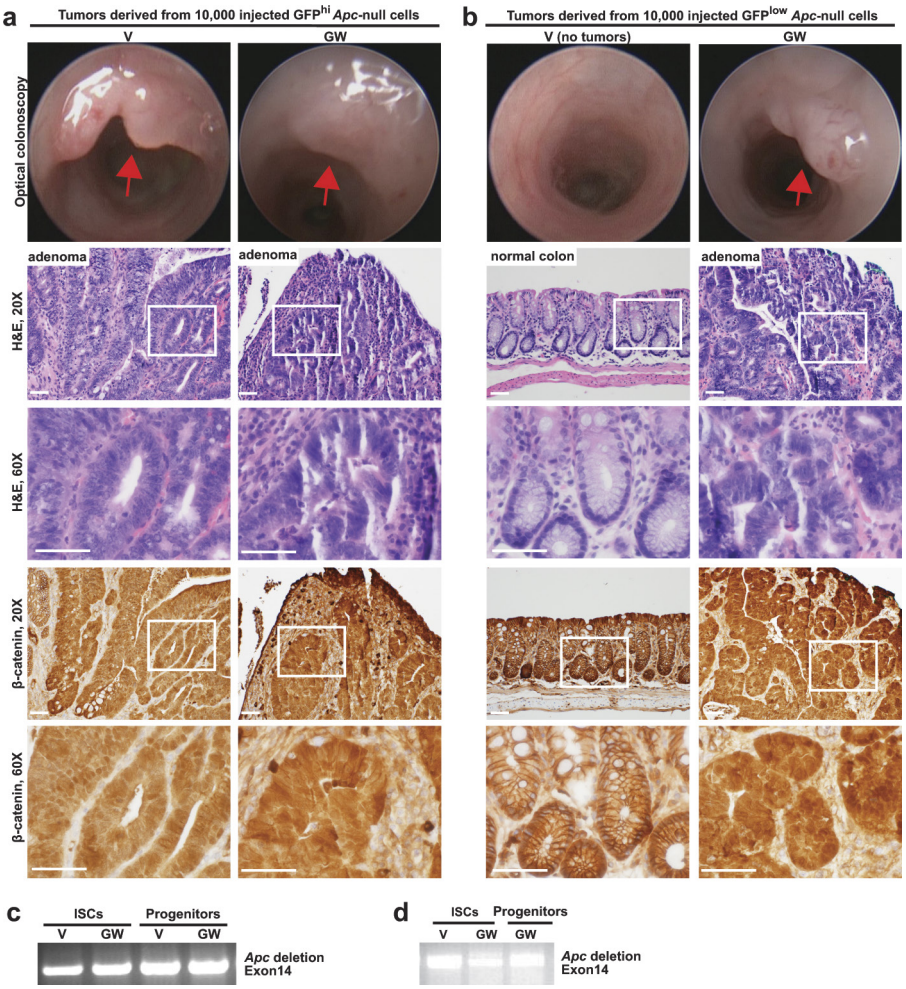

Extended Data Figure 10 | PPAR-δ activation bestows adenoma-initiating capacity to *Apc*-null progenitors. a, **b**, Representative optical endoscopy images (top) from Fig. 5, with H&E (middle) and β-catenin (immunohistochemistry, bottom) sections of adenomas derived from orthotopic transplantation of *Apc*-null ISCs (**a**, Lgr5-GFP^{hi}) and progenitors (**b**, Lgr5-GFP^{low}) from vehicle- and GW501516-treated mice 4 days after *Apc* deletion. Tumours exhibited hyperchromasia, lack of maturation, nuclear crowding and nuclear β-catenin positivity. Two independent pathologists blinded to treatment groups interpreted the results. **c**, **d**, *Apc* deletion was confirmed in sorted small intestinal ISCs and progenitors from vehicle- and GW501516-treated *Apc*$^{L/L}$; *Lgr5-EGFP-IRES-CreERT2* mice 4 days after tamoxifen administration (**c**, $n = 3$) and in isolated tumours (**d**, $n = 3$) by PCR amplification, using allele-specific deletion primers targeting exon 14. Unless otherwise indicated, n represents independent experiments. Scale bars (**a**, **b**), 50 μm (20×) and 20 μm (60×).